



## REVIEW

# Recent advances in nano-photocatalysts for organic synthesis



N.P. Radhika<sup>a,\*</sup>, Rosilda Selvin<sup>b,\*</sup>, Rita Kakkar<sup>a</sup>, Ahmad Umar<sup>c,\*</sup>

<sup>a</sup> Department of Chemistry, University of Delhi, Delhi 110007, India

<sup>b</sup> Department of Chemistry, King Abdulaziz University (Girls Campus), Jeddah 21589, Saudi Arabia

<sup>c</sup> Department of Chemistry, Faculty of Science and Arts and Promising Centre for Sensors and Electronic Devices (PCSED), Najran University, Najran 11001, Saudi Arabia

Received 24 April 2016; accepted 17 July 2016

Available online 2 August 2016

## KEYWORDS

Photocatalysis;  
Nano-photocatalysis;  
Organic synthesis;  
Green Chemistry;  
Photosensitization

**Abstract** This review seeks to explore the literature pertaining to the applicability of nano-photocatalysts in fine chemical synthesis of organic compounds. The current methods of preparation of organic compounds in laboratories and industries are highly demanding on the non-renewable sources of energy. These conventional methods also generally require extreme conditions of temperature and pressure. Owing to deeper global awareness toward conservation of non-renewable sources of energy, there has been a shift of focus toward photocatalysis in the recent years. Photocatalysts are long known to catalyze various organic reactions such as oxidation, reduction, addition, cyclization and decomposition. The advent of nanotechnology made it possible to scale down these photocatalytic materials from bulk- to nano-scale and thereby further widen their scope and efficiency. Advances in material chemistry and nanotechnology have also made it possible to synthesize nanophotocatalysts of new genres, properties of which can be controlled and designed at molecular level. In this review, an attempt has been made to classify these diverse nanophotocatalysts into different groups, based on their composition and mechanism. Since the literature survey revealed that the chemoselectivity and efficiency of the nanophotocatalysts depend on their method of preparation, an overview of their common synthesis protocols is included. The review also highlights the various organic conversions for which these nanomaterials can be used under UV/visible irradiation. Nanophotocatalysts hold a great promise for environmentally-benign synthesis of highly useful organic compounds. We believe that this review

**Abbreviations:** GR, graphene; RGO, reduced graphene oxide; GO, graphene oxide; SEG, solvent exfoliated graphene; DFT, density functional theory; NSP, nanosphere;  $e^-h^+$ , electron-hole pair; SPR, Surface Plasmon Resonance; LSPR, Localized Surface Plasmon Resonance; HT, hydrothermalite; MOF, metal-organic framework.

\* Corresponding authors.

E-mail addresses: [radhika.rjsh@gmail.com](mailto:radhika.rjsh@gmail.com) (N.P. Radhika), [selvinrosilda@yahoo.com](mailto:selvinrosilda@yahoo.com) (R. Selvin), [ahmadumar786@gmail.com](mailto:ahmadumar786@gmail.com) (A. Umar).

Peer review under responsibility of King Saud University.



Production and hosting by Elsevier

can provide insights into research done in this field so far, which can pave way for further progress in this topic of far-fetched social significance.

© 2016 The Authors. Production and hosting by Elsevier B.V. on behalf of King Saud University. This is an open access article under the CC BY-NC-ND license (<http://creativecommons.org/licenses/by-nc-nd/4.0/>).

## Contents

1. Introduction . . . . .	4551
2. Semiconductor-based nanophotocatalyst . . . . .	4552
2.1. Graphene-semiconductor nanocomposite . . . . .	4552
2.1.1. Preparation of graphene-semiconductor nanocomposite . . . . .	4552
2.1.2. Mechanism of photocatalytic activity for organic synthesis by graphene-semiconductor nanocomposite . . . . .	4556
2.1.3. Selective organic transformations photocatalyzed by graphene-semiconductor nanocomposites . . . . .	4556
2.2. Other modified semiconductor materials as nanophotocatalysts for organic synthesis . . . . .	4561
2.2.1. Nanocomposite of two semiconductors . . . . .	4561
2.2.2. Core-shell nanocomposite . . . . .	4561
2.2.3. Non-metal doped semiconductor material. . . . .	4562
2.2.4. Metal-modified semiconductor. . . . .	4563
3. Surface Plasmon Resonance-mediated nanophotocatalyst . . . . .	4565
3.1. Mechanism of photocatalytic activity for the organic synthesis by LSPR . . . . .	4565
3.2. Preparation of surface plasmon mediated photocatalyst . . . . .	4565
3.3. Selective organic transformations photocatalyzed by surface plasmon mediated catalyst . . . . .	4566
3.3.1. Selective oxidation reactions . . . . .	4566
3.3.2. Selective reduction reactions . . . . .	4567
3.3.3. Addition reaction . . . . .	4568
4. Metal-organic charge-transfer based nanophotocatalyst: MOF . . . . .	4568
4.1. Mechanism of photocatalytic activity for organic synthesis by MOF . . . . .	4569
4.2. Selective organic transformations photocatalyzed by MOF . . . . .	4571
5. Conclusions and perspectives . . . . .	4572
References . . . . .	4572

## 1. Introduction

A catalyst is a substance that alters the rate of a reaction without being consumed in the reaction. If such an alteration in the rate of the reaction by the catalyst requires the presence of light, then it is said to be a photocatalyst.

Photocatalysts can catalyze reactions in which the substrate is already photochemically active or reactions in which the substrate is otherwise photochemically inactive. The later implies photosensitized reactions in which the catalyst absorbs photons when then cause electronic excitations within the catalyst. This creates energy-rich states of electron-hole pairs. The catalyst then drives photochemically inactive reactions either by the transfer of energy to the substrate or by acting as a donor or an acceptor of electron (Larson et al., 1992; Neubauer et al., 2014).

An important photocatalytic reaction that occurs in nature is photosynthesis. A major breakthrough in carrying out photocatalytic reactions in a controlled manner in laboratory was the report by Fujishima and Honda (1972). In this study, TiO<sub>2</sub> was used as a photocatalyst to split water into hydrogen and oxygen, under UV irradiation. Since then, many photocatalysts such as TiO<sub>2</sub>, TiO<sub>2</sub>-RuO<sub>2</sub> powders, mercuric thiocyanate, ruthenium(III) complexes, ZnO, Fe<sub>2</sub>O<sub>3</sub>, ZnS and CdS (Bandara et al., 1999; Bickley et al., 1973; Harada et al., 1989; Hubesch and Mahieu, 1985; Inoue, 2009; Kawai and Sakata, 1980; Matsumura et al., 1984; Tennakone, 1985; Tian et al., 2012) have been studied widely for various reactions.

Progress in nanotechnology further led to the development of new types of photocatalysts. Photocatalysts of the same material in the nano-form show quite different properties from the bulk state. This can be ascribed to surface size effect and quantum confinement (Nedeljkovic et al., 1986; Roduner, 2006). In fact, these effects bestow the nanophotocatalysts with certain advantages over the bulk materials:

- (i) High surface area to volume ratio which leads to a high fraction of particles and hence a high fraction of active sites, on the surface of the catalyst (Poole and Owens, 2003).
- (ii) Dependence of the valence band-conduction band energy gap on the size of nanoparticles. This makes it possible to tune the wavelength at which the material absorbs, by changing the size of the nanocatalyst. Thus, the electronic and optical properties of the catalyst could be further modified by changing the size of nanoparticles (Hoffman et al., 1992; Kumar et al., 2011; Matsumura et al., 1985).

Because of these conducive properties, nanophotocatalysts find applications in wide range of reactions such as in splitting of water to generate hydrogen fuel, in dissociation of volatile organic pollutants, in degradation of dyes, in inactivation of cancer cells and in organic synthesis (Curri et al., 2003; Kaur et al., 2013; Maeda and Domen, 2010; Mangrulkar et al., 2012; Rozhkova et al., 2009; Sathishkumar et al., 2011; Somorjai et al., 2009; Townsend et al., 2012). In earlier years of development of nanophotocatalysts, studies

focused more on their applications in degradation of dyes and pollutants and in splitting of water. More recently, nanophotocatalysts are being progressively considered for catalyzing various organic reactions, which can provide a Green Chemistry alternative to the conventional methods employed in laboratories and industries that use thermal energy for the same.

Novel nanophotocatalysts are being developed with an objective to harness solar energy to synthesize organic compounds under controlled conditions. This review focusses on the recent advances in preparation and applications of such nanophotocatalysts. An attempt has been made to systematically organize the plethora of nanophotocatalysts that have been reported for organic synthesis, on the basis of their mechanism of action. The catalysts have thus been classified into semi-conductor, plasmon-mediated and metal-organic framework based materials. A summary of the synthesis routes employed for the preparation of these nanophotocatalysts has been included in cases where the activity of nanophotocatalysts was found to be dependent on their synthesis strategy. The following sections comprehensively discuss each of these photocatalytic materials in detail.

## 2. Semiconductor-based nanophotocatalyst

Semiconductor-based materials have been extensively studied for their applications in bringing about organic reactions photo catalytically. On irradiating a semiconductor, it absorbs photons. These photons cause the promotion of electrons from valence band to conduction band in the material. The electron-hole pair ( $e^-h^+$ ) so-generated may recombine leading to dissipation of light energy as heat or may interact with electron acceptors and donors adsorbed on the surface, causing their chemical transformations.

Different semiconductors (e.g.  $TiO_2$ ,  $ZnO$ ,  $\alpha-Fe_2O_3$  and  $WO_3$ ) have been considered for their potential use as photocatalysts. Out of these, the most widely studied semiconductor for heterogeneous photocatalysis is  $TiO_2$  because of its high stability, low toxicity, chemical inertness and resistance to photocorrosion (Fujishima et al., 2000). But the large band gap of  $TiO_2$  (3.0–3.2 eV) causes an absorption in the UV region. Since UV forms only 5–8% of the spectrum of sunlight, studies were done to develop photocatalysts that can absorb preferentially in the visible region.

CdS photocatalyst was reported to be an alternative to  $TiO_2$  as CdS band gap is lower (2.4 eV). On the flipside, photoactivity of CdS is restrained by high frequency of recombination of photo-induced electron-hole pairs and by photo-corrosion. To overcome these drawbacks of  $TiO_2$  and CdS in particular and of semiconductors in general, principles of nanotechnology and catalysis have been integrated to develop nano-scale composites of semiconductors with other materials. The idea is to engineer semiconductor-based materials to develop photocatalysts that possess high surface area, absorb more in the visible region of spectrum and photo-generate more stable electron-hole pairs. Such composites have been prepared by assembling semiconductors with graphene, other materials of semiconductor family, metals or non-metals. Nano-composites with core@shell morphology have also been probed for organic synthesis. The following sub-sections further examine these nanocomposites.

### 2.1. Graphene-semiconductor nanocomposite

Graphene (GR) is defined as “A single carbon layer of the graphite structure”, the nature of which can be described “by

analogy to a polycyclic aromatic hydrocarbon of quasi infinite size” (McNaught and Wilkinson, 1997). It is a 2-D crystalline allotrope of carbon having hexagonal pattern of  $sp^2$  hybridized carbon. It was first synthesized by Novoselov et al. in 2004. The preparation involved mechanical exfoliation from bulk graphite (Novoselov et al., 2004). Graphene has unique properties such as large surface area, high mechanical strength, high electrical conductivity, high electron mobility and high elasticity (Kuzmenko et al., 2008; Novoselov et al., 2004; Stoller et al., 2008). The nanocomposites of graphene or reduced graphene oxide (RGO) with semiconductors such as metallates, metal oxides or metal sulfides can potentially improve the photocatalytic ability of the semiconductor.

#### 2.1.1. Preparation of graphene-semiconductor nanocomposite

Graphene-semiconductor nanocomposites comprise of semiconductor nanoparticles homogeneously anchored to 2-D graphene. The precursor for graphene may be either pristine graphene (GR) or graphene oxide (GO). Graphene composites have been proved to show better photocatalytic performance than the composites of semiconductor with the other carbon-based material, carbon nanotube. In fact, a comparison between the two nanostructures GR- $TiO_2$  and CNT- $TiO_2$  (CNT-carbon nanotube) revealed benefits of GR over CNT. Compared to CNT, GR facilitated better control of the morphology of nanocomposite and provided greater improvement in the photocatalytic efficiency of  $TiO_2$  (Y. Zhang et al., 2011). Yet the primary criterion for a composite to show good catalytic performance is a good interfacial association between the components, which will further depend on the precursors of the components and the route adopted to anchor the components on each other.

So, even though there are no doubts on the plausibility of improved catalytic ability of the graphene-semiconductor composites, the source of graphene itself is of profound significance. If GR is used, graphene sheets tend to get aggregated. Also, when GR is used, the interfacial interaction between the resultant graphene and semiconductor in the composite is found to be limited. To strengthen the graphene-semiconductor interactions, additional steps need to be incorporated in the synthesis route whereby suitable functional groups are introduced in the structure (Bai et al., 2011; Hsiao et al., 2010; Wajid et al., 2012).

Another alternative is the use of solvent (N,N-dimethylformamide)-exfoliated GR (SEG) as the precursor of graphene (Liang et al., 2011; Y. Zhang et al., 2012b). But, due to the deficiency of hydrophilic groups in SEG, film forming polymers such as polyvinylpyrrolidone or ethyl cellulose need to be used to promote the interfacial contact of SEG with the semiconductor.

Yet another graphene precursor that is generally employed is graphene oxide (GO). It is usually prepared by the modified Hummers' method. Unlike SEG, the abundance of oxygen on GO ensures a good interfacial contact with the semiconductor. As a matter of fact, analysis of graphene oxide by Raman spectra, X-ray diffraction pattern, Fourier transform infra-red spectra, zeta potential analysis and X-ray photoelectron spectra suggests that GO sheet contains large number of functional groups on its surface, such as epoxide group, carbonyl group, hydroxyl group and carboxyl group (Krishnamoorthy et al., 2013). Therefore, additional steps or agents are not required

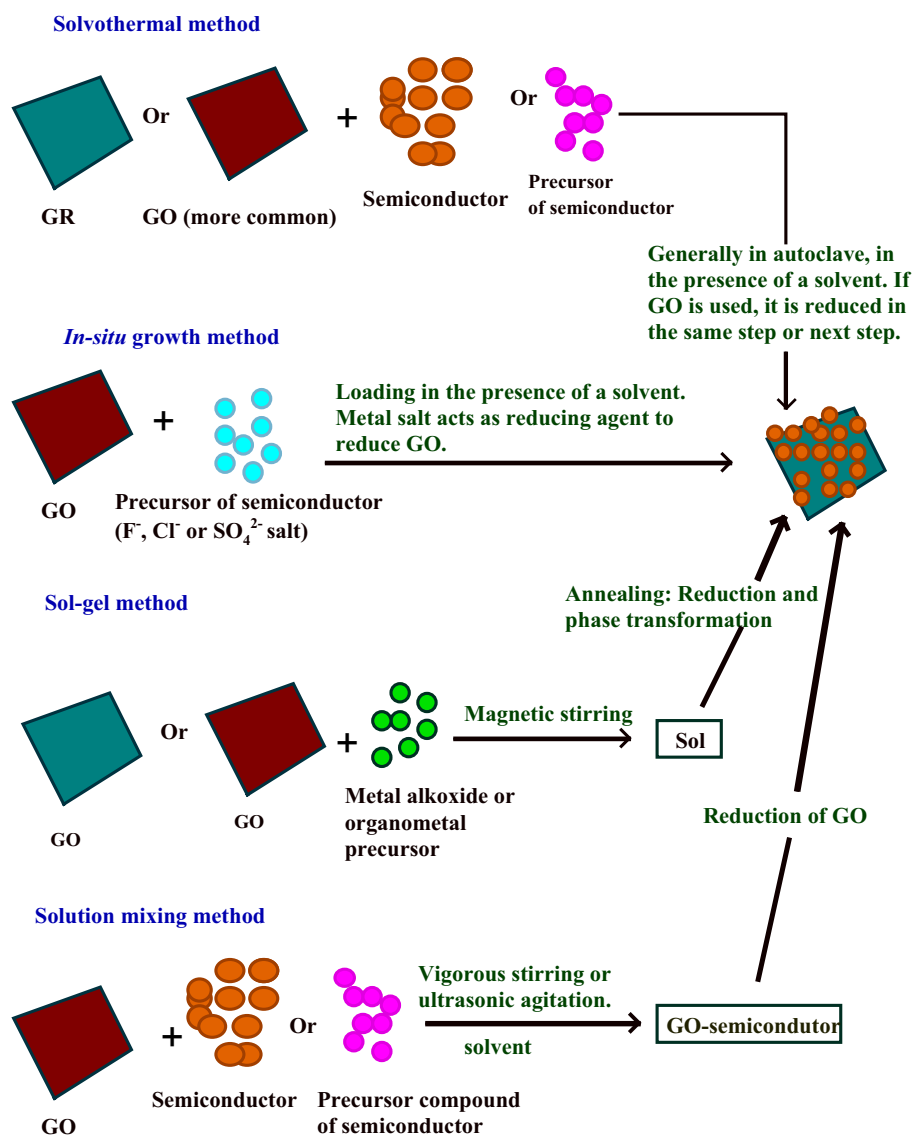


**Figure 1** Major synthetic routes to fabricate graphene-semiconductor nanocomposites.

to stabilize the composite (Huang et al., 2010; Kamat, 2010; Lightcap et al., 2010; Park et al., 2009; Sun et al., 2011; Tung et al., 2011; Y. Zhang et al., 2011).

But the main drawback in the use of GO is the large number of defects that are introduced when it is prepared by modified Hummers' method due to strong oxidation steps. In this context, SEG-TiO<sub>2</sub> catalyst is better as it has a lower defect density than GO-TiO<sub>2</sub> composite (Liang et al., 2011). Also, in all cases in which GO is not reduced in situ during the course of preparation of its nanocomposite with the semiconductor, it is mandatory to add steps to reduce it. This is usually achieved by chemical reduction or by heating. Therefore, the nanocomposites effectively obtained are semiconductor-reduced graphene oxide (RGO) composites (Lightcap et al., 2010). If reduction is not done, then, GO, due to its comparatively low electrical conductivity, will not be able to extend the lifetime of electrons and holes generated for them to be of any practical use.

After graphene is procured, its nanocomposite with the semiconductor is prepared most commonly by solvothermal, in situ growth, solution-mixing or sol-gel method. These different synthetic routes are diagrammatically compared in Fig. 1.

In solvothermal method, as discussed in the previous paragraph, if graphene oxide is used as precursor, then it may get reduced simultaneously (one pot solvothermal process) or may have to be reduced in a subsequent step (Jianwei et al., 2013). Solvothermal method was successfully employed to prepare TiO<sub>2</sub>-GR (Zhang et al., 2010), GR-Bi<sub>2</sub>WO<sub>6</sub> (Gao et al., 2011), Pt-GO-TiO<sub>2</sub> (Neppolian et al., 2012), GR-CdS (Q. Li et al., 2011; Ren et al., 2014), GO/ZnS (J. Wu et al., 2010), GR-ZnO (Kamat and Patrick, 1992; Williams and Kamat, 2009), TiO<sub>2</sub>-RGO (He et al., 2016; Shen et al., 2011; Shu et al., 2013) and sandwich-like hetero structures of the form MO/G/MO (M = Ti, Zn, Mn, Cu or Zr) (Zou et al., 2011). Shen et al. (2011) used ascorbic acid as reducing agent in hydrothermal synthesis of TiO<sub>2</sub>-RGO composite from GO

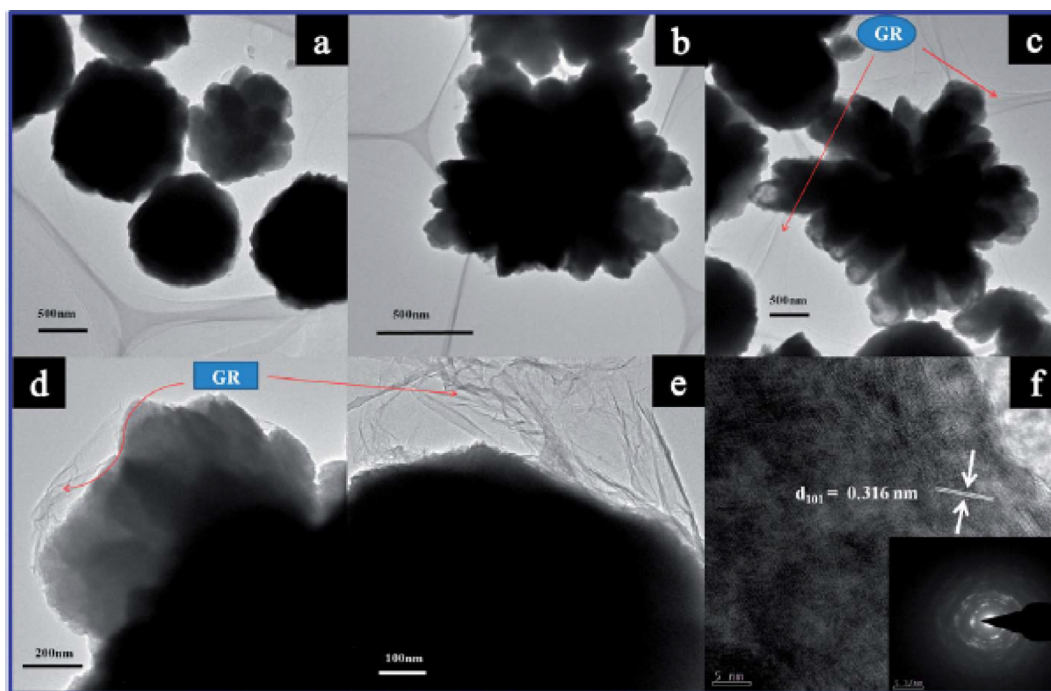


**Figure 2** TEM images of blank CdS (a and b), (c–e) TEM images and (f) HRTEM images of the 5% GR–CdS nanocomposite with the SAED pattern in the inset (Ren et al., 2014).

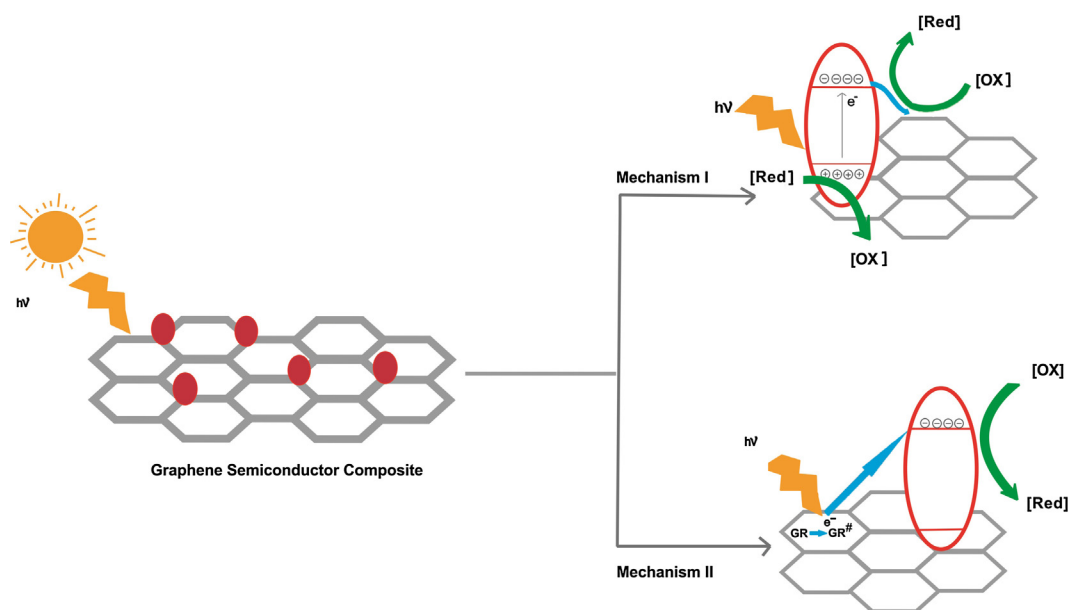


**Figure 3** Illustration of mechanism of photocatalytic activity of graphene-semiconductor nanocomposite: [Ox] and [Red] indicate oxidized and reduced species respectively.

sheet. A nanocrystal seed directed hydrothermal reaction was reported by Zou et al. (2011) to prepare sandwich-like heterostructures of the form MO/G/MO ( $M = \text{Ti, Zn, Mn, Cu}$  or  $\text{Zr}$ ). In another research, GR-ZnO nanocomposite for Atomic Force Microscopy (AFM) studies was prepared by drop casting dilute mixtures of ZnO nanoparticles and GO sheets in ethyl alcohol onto mica substrates (Williams and Kamat, 2009). Size of ZnO nanoparticles could be tuned in

the size-quantized regime (2–5 nm) by adjusting the hydrolysis temperature in their preparation stage (Kamat and Patrick, 1992).

In in situ method, a precursor of the semiconductor, which generally is a metal salt, is mixed with precursor of graphene. On mixing, the nucleation and growth of semiconductor on graphene precursor in nano-dimensions take place (Jianwei et al., 2013). In situ synthesis was used to prepare

graphene-based TiO<sub>2</sub> composite in aqueous medium using different precursors, TiCl<sub>3</sub> (C. Zhu et al., 2010), TiF<sub>4</sub> (Lambert et al., 2009) and Ti(SO<sub>4</sub>)<sub>2</sub> (Ding et al., 2011; Q. Zhang et al., 2011). Graphene Oxide intercalated composite (TiO<sub>2</sub>-GO) was prepared at 80 °C, using GO and Ti(SO<sub>4</sub>)<sub>2</sub> (Q. Zhang et al., 2011). Jiang et al. (2012) used SnCl<sub>2</sub>·2H<sub>2</sub>O as metal salt precursor for preparing SnS<sub>2</sub>-graphene in aqueous medium. In cases where GO is used, its reduction can also take place in situ (Chen et al., 2012; J. Zhang et al., 2011). For instance, J. Zhang et al. (2011) prepared RGO-TiO<sub>2</sub> and RGO-SnO<sub>2</sub> nanocomposites using TiCl<sub>4</sub> and SnCl<sub>2</sub> as precursors respectively. In these cases, the metal salts also acted as reducing agents. On the other hand, in the preparation of TiO<sub>2</sub>-GR nanocomposite from TiCl<sub>4</sub> and GO sonochemically, hydrazine was used as reducing agent (J. Guo et al., 2011). A template may also be needed to direct the growth of semiconductor nanoparticles on graphene. For instance, J. Du et al. (2011) used polystyrene colloidal spheres as templates in preparing hierarchically ordered TiO<sub>2</sub>-graphene composite films. On the other hand, N. Li et al. (2011) reported the self-assembly of uniform mesoporous anatase TiO<sub>2</sub> on graphene sheets. This self-assembly of nanospheres of anatase TiO<sub>2</sub> took place in the absence of any template.

In solution-mixing method, precursor of semiconductor is agitated with GO by vigorous stirring or ultrasonic agitation, followed by reduction and drying or calcination. The experimental conditions are milder compared to the hydrothermal method, but the interfacial contact between GO and semiconductor may be rendered lower than that in the composite prepared by solvothermal method (Jianwei et al., 2013). There is a wide range of nanocomposites prepared by this method. This includes ZnFe<sub>2</sub>O<sub>4</sub>-ZnO nanocomposites immobilized on graphene (Sun et al., 2013), SnO<sub>2</sub>-GR (Paek et al., 2009), GR-CdSe quantum dots (Geng et al., 2010), Sr<sub>2</sub>Ta<sub>2</sub>O<sub>7-x</sub>N<sub>x</sub>-GR (Mukherji et al., 2011), GO-gC<sub>3</sub>H<sub>4</sub> (where g-C<sub>3</sub>H<sub>4</sub> denotes graphite like C<sub>3</sub>H<sub>4</sub>) (Liao et al., 2012) and ZnO-GR (Xu et al., 2011). Graphene sheet itself may be obtained from natural graphite using a high pressure ultrasonic reactor (Stengl et al., 2011). The graphene so prepared has lower number of defects compared to graphene oxide prepared by Hummers' method.

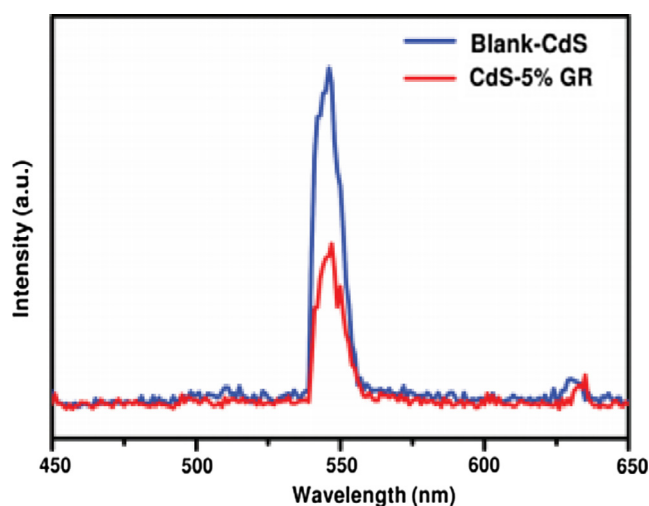


**Figure 4** Photoluminescence spectra of blank CdS and 5% GR-CdS (N. Zhang et al., 2011c).

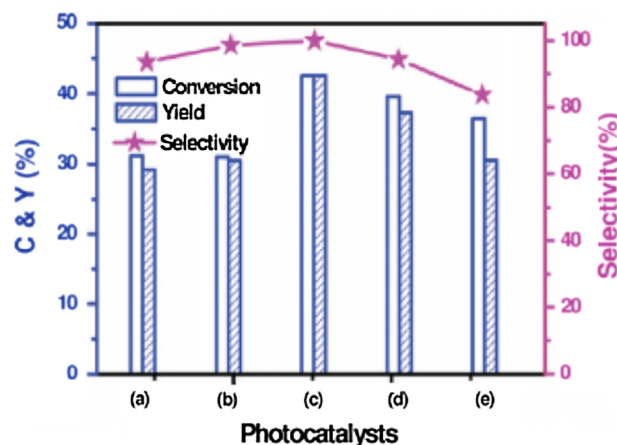


**Figure 5** Photocatalytic oxidation of benzyl alcohol to benzaldehyde under visible irradiation of 4 h over different nanocomposites (a) blank-CdS, (b) CdS-1% GR, (c) CdS-5% GR, (d) CdS-10% GR, and (e) CdS-30% GR (N. Zhang et al., 2011c).

Sol-gel method provides a route to prepare nanocrystalline semiconductor metal oxide from metal alkoxide or an organometal. When a metal alkoxide or an organometal is added to graphene and magnetically stirred in the presence of a dispersion medium such as ethyl alcohol, a sol is formed. On heating and drying, the sol undergoes series of polycondensation and phase transformation, following which semiconductor nanoparticles get homogeneously anchored on graphene sheets. The method was applied to prepare TiO<sub>2</sub>-GR nanocomposite using titanium(IV) butoxide as the Ti source and ethanol as solvent (Wojtoniszak et al., 2012).

CdS-GR nanocomposite was synthesized by a single-step process, by reacting GO, thioacetamide, CdCl<sub>2</sub> and poly (vinyl pyrrolidone) at 80 °C for 2 h (Zhao et al., 2012). In another work, ZnS-GR nanocomposite was synthesized by the reaction of ZnCl<sub>2</sub> with Na<sub>2</sub>S in a GO aqueous medium at room temperature (Y. Zhang et al., 2012a).

Another synthetic route is ex situ hybridization. In this method, conditions are provided to bind together graphene-based nanosheets and pre-synthesized nanocrystals. This binding is by chemical bonding or non-covalent interactions. In order to promote the interfacial interactions, either structural alteration of the nanocrystals and/or graphene sheets is done or an adhesive polymer like Nafion is used. Sun et al. (2010) reported the preparation of one such nanocomposite, Nafion-coated TiO<sub>2</sub>-RGO.

In addition to the above methods, other techniques such as Chemical Vapor Deposition (CVD), Atomic Layer Deposition (ALD), Electrochemical Deposition (ED), Electrostatic Self-Assembly coupled hydrothermal reduction and Microwave-assisted reaction have also been reported to prepare the nanocomposites. CVD method was used to synthesize CoS-GR nanocomposite (Bi et al., 2013; S. Das et al., 2012). ALD method was used to prepare TiO<sub>2</sub>-GR nanosheet (Meng et al., 2011). Electrochemical Deposition method was used to deposit a ZrO<sub>2</sub>-GR nanocomposite on Glass Carbon Electrode (D. Du et al., 2011). Other nanocomposites prepared by this method are ZnO, Cu<sub>2</sub>O and CdSe (quantum dots) on RGO or graphene films (Kim et al., 2010; S. Wu et al., 2010; Yin et al., 2010). Recently, 1-D-2-D (CdS nanowires-RGO)

composite structures were developed by electrostatic self-assembly followed by hydrothermal reduction (S. Liu et al., 2013). Another CdS based nanocomposite, CdS-RGO was prepared by a one-step microwave assisted irradiation technique (Liu et al., 2011). F.-J. Chen et al. (2013) reported a novel room-temperature solid-state route for preparing metal sulfide-GO nanocomposite. Qiu et al. (2015) developed a one-step vacuum activation technique to prepare  $\text{Ti}^{3+}$  self-doped  $\text{TiO}_2$ -graphene nanosheet photocatalyst. The technology involved activation of a mixture of GO and commercial  $\text{TiO}_2$  in vacuum at  $300^\circ\text{C}$  for 3 h. This single step could serve multiple purposes – GO was reduced to GR, self-doping of  $\text{Ti}^{3+}$  took place and  $\text{TiO}_2$  nanoparticles were loaded on GR surface.

The significance of the method chosen to synthesize the nanocomposite photocatalyst cannot be underestimated. The method of synthesis has a profound impact on the catalytic activity of the photocatalyst (Ren et al., 2014). A comparison of the 5% GR-CdS catalyst prepared by different routes, toward selective oxidation of benzyl alcohol to benzaldehyde indicates an increase in activity in the order: GR/CdS-I (composite prepared by in situ synthesis), GR/CdS-E (composite prepared by electrostatic self-assembly) and GR/CdS-H (composite prepared hydrothermally). The experimental conditions were identical and the catalysts differed only in the synthesis route that was employed to fabricate them. The trend indicates that the composite prepared hydrothermally was most efficient. It can thus be conclusively pointed out that the association between GR and CdS was greatest in the catalyst prepared by hydrothermal synthesis. Transmission Electron Microscopy (TEM) images also depict this close GR-CdS interaction in the composite prepared hydrothermally (Fig. 2).

### 2.1.2. Mechanism of photocatalytic activity for organic synthesis by graphene-semiconductor nanocomposite

There are two broadly plausible mechanisms to explain the enhancement in photoactivity of semiconductor on incorporating graphene (Fig. 3). According to the first proposed mechanism (An and Yu, 2011; Chen et al., 2010; Long et al., 2013; Ng et al., 2010; Xiang and Yu, 2013), the semiconductor absorbs photons of wavelength corresponding to the energy gap between valence and conduction band. This leads to excitation of electrons from the valence band to the conduction band, leaving behind holes. These electrons and holes then selectively reduce or oxidize a substrate adsorbed on the nanocomposite. The presence of graphene enhances the photocatalytic activities of the nanocomposite in the visible part of the spectrum due to following reasons:

- (i) The interaction between semiconductor and graphene leads to M–C or M–O–C bonds, where M represents the metal. These interactions can lead to new energy levels. For instance, in RGO composites prepared from GO precursors, deoxygenation of GO takes place as it undergoes reduction to RGO. To balance this, as the growth of semiconductor nanoparticle proceeds, the surface lattice oxygen atoms tend to diffuse out from the semiconductor and chemically interact with RGO. Therefore, oxygen vacancies are created in the semiconductor, which lead to the creation of new energy levels lower than the conduction band. This reduces the energy gap in semiconductor, leading to red shift. Hence, greater quantum efficiency in visible part of the spectrum results (Chen et al., 2010).
- (ii) The high conductivity and electron mobility of graphene increase the recombination time and lead to greater stability of photogenerated holes and electrons (An and Yu, 2011; Long et al., 2013; Ng et al., 2010) which otherwise would have recombined in few nanoseconds. Thus, the mean free path of electrons is increased, whereby the electrons can be conducted over a larger area in the carbon framework, increasing the possibility of its interaction with substrates.
- (iii) Graphene acts as a support and enhances the surface area of the photocatalyst. The interaction of 2-D conjugated  $\Pi$  electron system of graphene with the substrate increases the extent of adsorption of substrate on the nanocomposite.

The second proposed mechanism that is less widely studied was first reported experimentally by Y. Zhang et al. (2012a) for ZnS-GR system, on the basis of structure-photoactivity modifications and studies using scavenger radicals (Y. Zhang et al., 2012a). As per this proposal, the band gap in ZnS is large and it does not absorb in visible region, even after being anchored to graphene. Thus, the photoactivity is initiated by graphene rather than by the semiconductor. Graphene acts as a photosensitizer. It absorbs radiation and forms excited graphene,  $\text{GR}^\#$ .  $\text{GR}^\#$  then injects the photoexcited electron into the conduction band of the semiconductor. The subsequent trapping of this electron by oxygen leads to the production of superoxide radicals. These radicals then cause selective oxidation reactions (e.g. alkene to epoxide or alcohol to corresponding aldehyde). The role of graphene as a photosensitizer for the semiconductor is similar to that of an organic dye in dye-sensitized semiconductor or dye-sensitized solar cell. This can also be compared to photoinduced charge transfer from excited  $\text{C}_{60}$  to  $\text{TiO}_2$  (Kamat et al., 1997).

This idea of graphene as a photosensitizer has also been supported theoretically. For the first time, A. Du et al. (2011) did large-scale DFT calculations to study the graphene-rutile  $\text{TiO}_2$  interface charge transfers. It was proved that under visible light irradiation, excitation of electrons takes place from  $\Pi$  system of graphene to the conduction band of titania. This proposal clearly backs the second mechanism. Such an interface charge transfer leads to hole accumulation in graphene layer, that is analogous to p-type doping. This also shifts Fermi energy level 0.65 eV below the Dirac point in graphene-titania nanocomposite. As the electron-hole pair is now well-separated, the recombination rate of electron-hole pair is considerably lowered.

### 2.1.3. Selective organic transformations photocatalyzed by graphene-semiconductor nanocomposites

#### i. Selective oxidation reactions

The carbonyl compounds are chiefly used as precursors to synthesize other organic compounds, ranging from pharmaceuticals to flavoring agents to polymers such as plastics. The conventional industrial methods require the use of strong oxidizing agents such as permanganates or chromates and high temperature and pressure (Enache et al., 2006; Palmisano

et al., 2007; Sheldon et al., 2002; N. Zhang et al., 2011c). Nanophotocatalysts can be developed to conduct various oxidation reactions under milder conditions using  $O_2$  or  $H_2O_2$  as oxidizing agents (Maldotti et al., 2002; Ravelli et al., 2009). Different nanocomposites such as GR-CdS (N. Zhang et al., 2011c), cation modified GR-CdS (Zhang et al., 2014) and SEG-TiO<sub>2</sub> (Liang et al., 2011) have been studied for selective oxidation reactions. For example, CdS nanoparticles supported on 2-D graphene scaffold (GR-CdS) were used for oxidizing alcohols to aldehydes selectively (N. Zhang et al., 2011c). Various alcohols such as benzyl alcohol, derivatives of benzyl alcohol, cinnamyl alcohol and 3-methyl-2-buten-1-ol were oxidized in the presence of this catalyst. On carrying out the reaction under 300 W Xe lamp arc with UV cutoff wavelength  $\leq 420$  nm for 4 h, about 85% yield of aldehydes was obtained, which was about 20% higher than that using blank CdS. No heating to high temperature was required and  $O_2$  was introduced at an ambient pressure of 0.1 MPa. The reason for the increase in activity on integration of graphene into CdS can again be traced to the decreased recombination rate of photogenerated  $e^-h^+$  pair. This was further confirmed by the weak photoluminescence signal for 5% GR-CdS nanocomposite relative to blank CdS (Fig. 4). The conversion rate and selectivity were highest when 5% GR-CdS nanocomposite was used (Fig. 5). The efficiency of these photocatalysts is quite comparable to that of some non-photocatalytic systems. For instance, in oxidation of benzyl alcohol to benzaldehyde, non-photocatalytic gold catalysts

gave 67% conversion after 6 h at 80 °C (Zhan et al., 2012). In the same reaction,  $MnO_2$  gave 37.7% conversion after 3 h at 80 °C (along with microwave irradiation) (Su et al., 2007). Another non-photocatalyst,  $CuMn_2$  mixed oxide nanoparticles could give a still better conversion (100%) in just 20 min at 102 °C (Ali et al., 2015). Yet, the importance of photocatalysts cannot be underestimated as they work at lower temperatures and utilize energy source that is available in abundance.

It is noteworthy that beyond this optimum value, a further increase in the concentration of GR decreases the selectivity toward aldehyde product. This may be because that higher concentration of graphene facilitates very strong interaction of the aldehyde with graphene, making it more difficult for desorption of the aldehyde to occur. As the aldehyde lingers on the catalyst for prolonged durations, probability of its getting further oxidized to benzoic acid or carbon dioxide increases manifold. Additionally, yield must have reduced at high graphene concentrations due to shielding effect and opacity of graphene, which in turn limit the absorption of light by CdS. Thus the amount of graphene in the composite should be optimum to render the catalyst most efficient under a set of conditions.

In 2014, with a view to further enhance its catalytic abilities, Zhang et al. modified graphene-CdS photocatalyst by incorporating small amounts of metal ions such as  $Ca^{2+}$ ,  $Cr^{3+}$ ,  $Mn^{2+}$ ,  $Fe^{2+}$ ,  $Co^{2+}$ ,  $Ni^{2+}$ ,  $Cu^{2+}$ , and  $Zn^{2+}$  (M) in the interfacial layer matrix between CdS and graphene (Zhang et al., 2014). The introduction of the metal was believed to offset

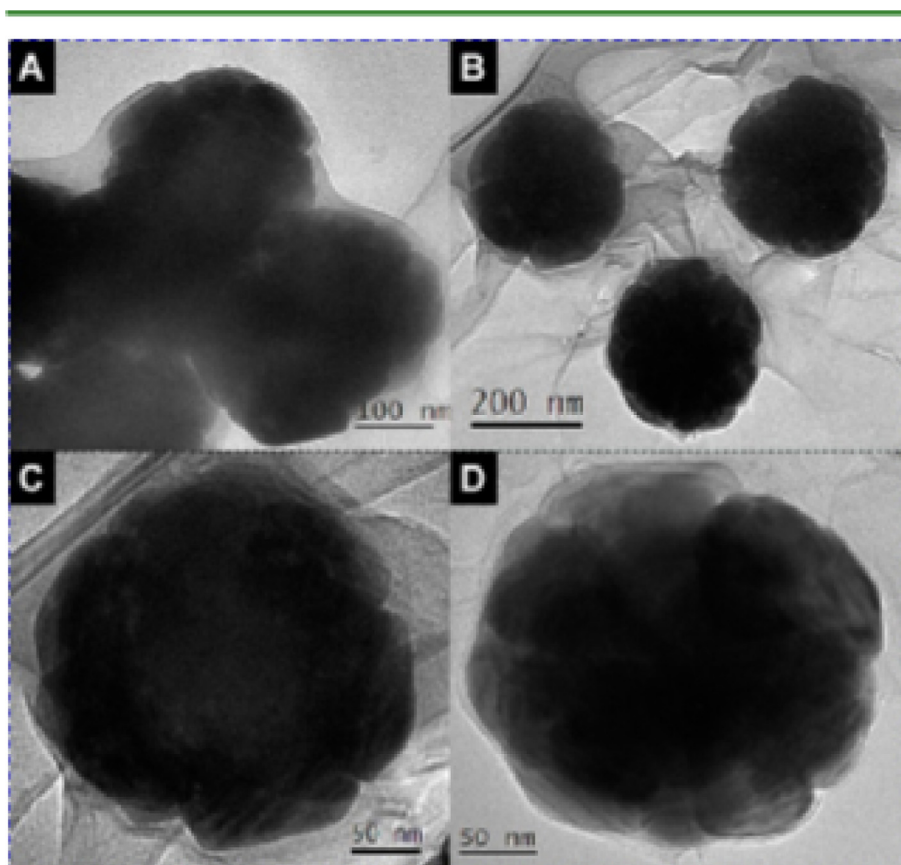


**Figure 6** TEM image of CdS NSPs/5% GR nanocomposite, with core@shell structures (Z. Chen et al., 2013).

the shielding effect of graphene and improve the semiconductor-graphene interfacial contact. The conversion of benzyl alcohol to benzaldehyde after 2 h of irradiation on using CdS-10% (GR-Ca) was about twice of that obtained using 5% GR-CdS as catalyst, under identical reaction conditions.

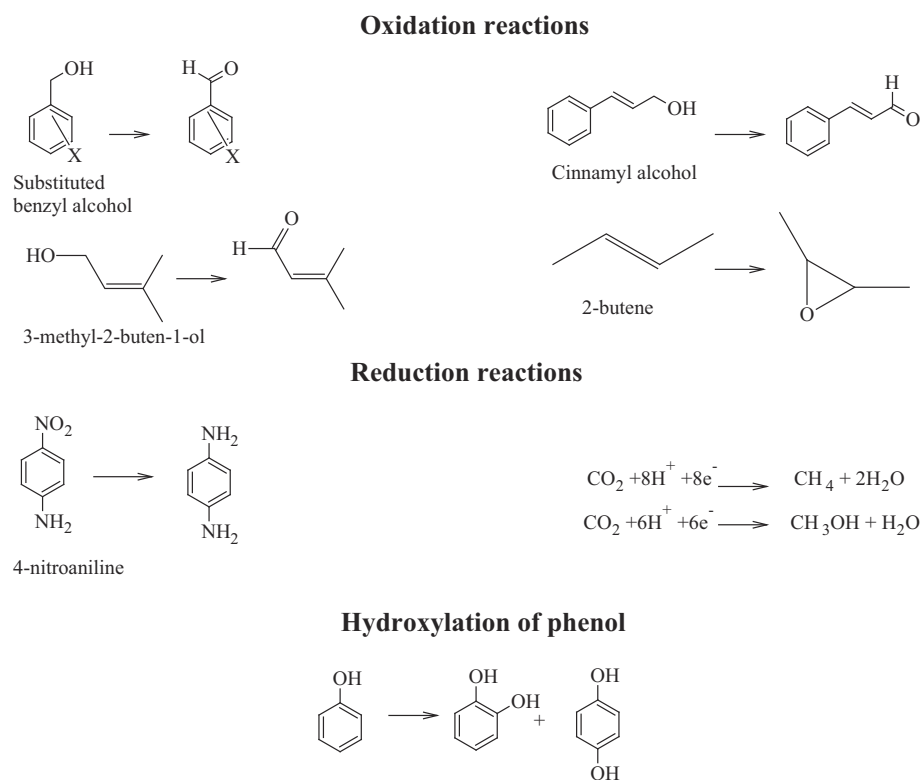
Generally, nanophotocatalyzed selective oxidation reactions are done using benzene trifluoride (BTF) as the solvent. Water is not used due to the difficulty in controlling the over-oxidation. Nevertheless, a novel nanocatalyst, SEG-TiO<sub>2</sub> was studied for the selective conversion of benzyl alcohol to benzaldehyde in water (Zhang et al., 2013). The catalyst was quite selective and didn't over-oxidize the aldehyde, even when reaction was done using water as a solvent. As discussed under preparation of graphene-semiconductor nanocomposites (Section 2.1.1), the usage of SEG instead of GO as graphene precursor lowered the defect density and thus improved the catalytic activity.

The merits of binary semiconductor-nanocomposite system were further strengthened by developing it into a ternary hybrid: CdS-GR-TiO<sub>2</sub> (N. Zhang et al., 2012). The ternary nanocomposite has been reported to be a more efficient photocatalyst compared to CdS-GR for the selective oxidation of benzyl alcohol to benzaldehyde, when irradiated by visible-light ( $\lambda > 420$  nm). The catalyst had maximum efficiency for the composition CdS-5% GR-10% TiO<sub>2</sub>. The determination of pore volume and pore size indicated that the introduction of the second semiconductor did not alter the morphology and the porosity of the nanocomposite. Despite this, the BET surface area of the ternary hybrid was detected to be larger than its foundation matrix CdS-5% GR. Thus the ternary

system could contribute more active sites for the adsorption of alcohol. Further, the band gap decreases from 2.36 eV (in CdS-graphene) to 2.26 eV in the ternary catalyst, leading to a favorable red shift. The mechanism proposed involves the excitation of electrons of CdS from the valence band to its conduction band. These are then transmitted from CdS to graphene and TiO<sub>2</sub>, leading to a longer electron transfer path. This results in an additional increase in the lifetime of photogenerated e<sup>-</sup>-h<sup>+</sup> pairs. The electrons then activate oxygen to superoxide radicals, which are good oxidizing agents. The holes in the valence band of CdS also oxidize the adsorbed alcohols.

D.P. Das et al. (2012) developed reduced graphene oxide-silver vanadate nanocomposite (RGO-Ag<sub>3</sub>VO<sub>4</sub>) photocatalyst for another oxidation reaction, 'photo-hydroxylation' of phenol to catechol, in the absence of H<sub>2</sub>O<sub>2</sub>. The reaction was done in aqueous medium and resulted in complete conversion. The selectivity toward catechol at room temperature under visible light irradiation within 2 h was 80.23% for 4RGO-Ag<sub>3</sub>VO<sub>4</sub> (corresponding to 4 wt.% C:Ag<sub>3</sub>VO<sub>4</sub>). The catalyst was quite stable and did not show leaching when photo-illuminated, that is otherwise characteristic to metal vanadates. The catalyst also showed superior performance as compared to non-photocatalytic material such as nano-sized hollow core mesoporous shell carbon loaded with transition metal (Jeong et al., 2005). This catalyst had been reported to give about 20–30% conversion, with 85% selectivity toward catechol and hydroquinone after 3 h of reaction, in the presence of H<sub>2</sub>O<sub>2</sub>.

Graphene acts as a photosensitizer in GR-ZnS nanocomposite and could catalyze selective oxidation of alcohols to aldehydes and epoxidation of alkene (Y. Zhang et al., 2012a).



**Scheme 1** Selective organic transformations catalyzed by graphene-semiconductor nanocomposites.

**Table 1** Photocatalytic selective oxidation of a series of alcohols into corresponding aldehydes over CdS nanowires and 1D CdS@TiO<sub>2</sub> under visible light ( $\lambda = 520 \pm 15$  nm) after irradiation for 8 h (Liu et al., 2012).

Entry	Substrate	Product	Conversion (%)		Yield (%)		Selectivity (%)	
			CdS	CdS@TiO <sub>2</sub>	CdS	CdS@TiO <sub>2</sub>	CdS	CdS@TiO <sub>2</sub>
1			13	34	12	33	97	97
2			7	41	4	30	60	74
3			21	39	8	25	36	65
4			7	30	5	21	73	70
5			4	38	3	33	88	87
6			6	37	5	36	97	96

## ii. Selective reduction reactions

A primary route to prepare amines is the reduction in nitro compounds. Amines, in turn are important precursors to synthesize dyes and drugs. These are also used for eliminating CO<sub>2</sub> and H<sub>2</sub>S from gas streams. For this reaction, alumina-supported hydrazine, in the presence of Fe(III) compounds is a non-photocatalyst that has given exemplary yield (89%) after 7 min of irradiation with microwave energy at 108 °C (Vass et al., 2001). Such high yields in short durations have not yet been attained in the presence of photocatalysts. But, research is being done in the field of photocatalysts with an objective to improve their performance. In particular, photocatalysts attract the attention of scientific fraternity for driving selective reduction in compounds such as 4-nitroaniline, for which non-photocatalytic systems have not been applied much.

Semiconductor-graphene nanocomposites have been studied as potential nanophotocatalysts for this reduction. The

reduction reactions, unlike selective oxidation reactions can be carried out more easily in aqueous medium under illumination of visible light. Usually, ammonium oxalate is used as hole quencher to reduce photocorrosion and nitrogen purge is used to prevent oxidation.

CdS nanoparticles based photocatalyst: CdS-GR was reported to be a better catalyst than blank CdS for the reduction in aromatic nitro compounds to corresponding amines (S. Liu et al., 2014). BET studies indicate a type II isotherm for blank CdS and a type IV isotherm for 5% CdS-GR composite, indicating a more porous structure of the composite.

CdS-GR nanocomposites can also be prepared by combining CdS nanowires with graphene (S. Liu et al., 2013) or by wrapping CdS nanospheres with graphene (Z. Chen et al., 2013). In the presence of this catalyst, the reduction in aromatic nitro compounds such as 2-nitroaniline and 4-nitrophenol indicated good yields of corresponding amine

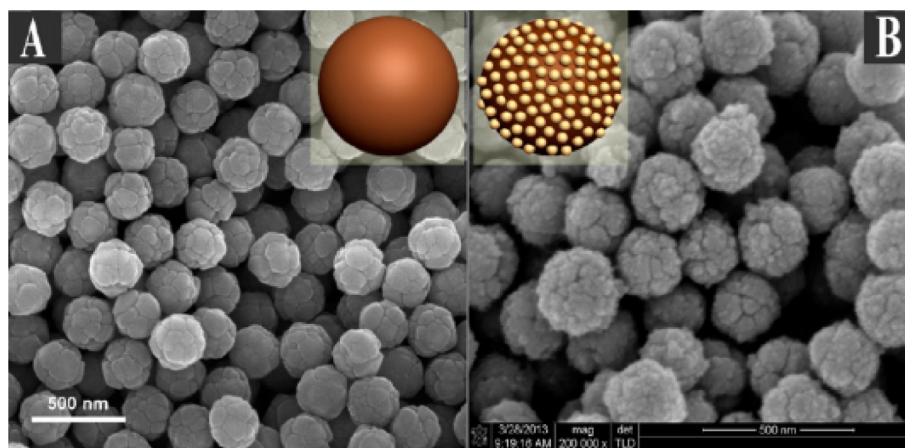
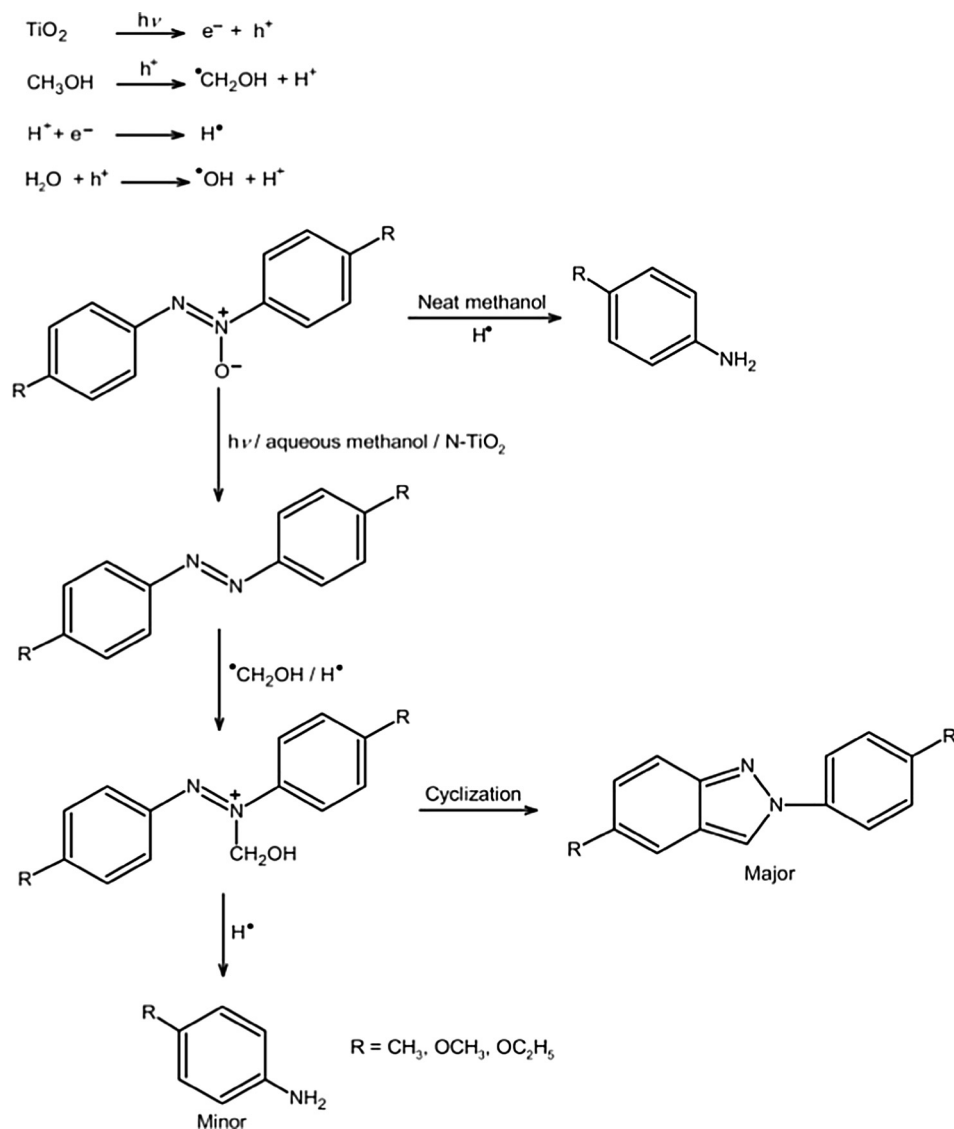


**Figure 7** SEM images of (A) bare CdS NSPs and (B) CdS NSPs@TiO<sub>2</sub> (the insets of A and B are the corresponding model illustrations) (Chen and Xu, 2013).



**Scheme 2** Possible reaction pathways for reductive cleavage of azoxybenzene on photoirradiation in the presence of nano N-TiO<sub>2</sub> (Selvam et al., 2012).

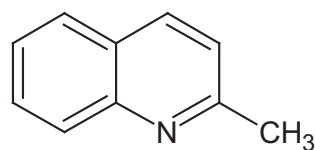
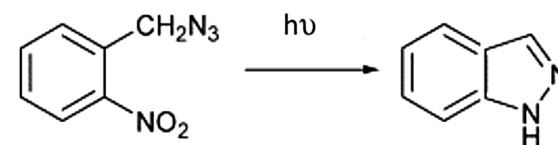
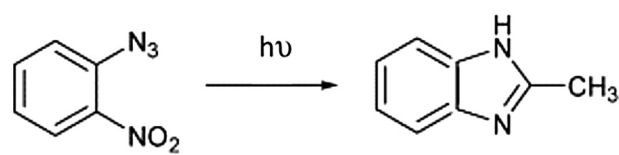


**Figure 8** Structure of quinaldine.

products. The catalyst gave higher yields for the reduction compared to blank CdS. TEM images indicated CdS NSPs wrapped by GR sheets have core@shell structures, with good interfacial contact between the two units (Fig. 6). The difference in the extent of conversion of alcohol using CdS NSPs/GR and using blank CdS increases as the reaction progresses for a greater duration.

The introduction of metal ions in the interfacial layer between graphene and CdS further increased the photoactivity (Zhang et al., 2014). The selective reduction of 4-nitroaniline anaerobically resulted in 80% conversion and 95% selectivity



**Scheme 3** Photocatalytic conversion using metal doped nano-TiO<sub>2</sub> (a) 2-nitrophenyl azide to 2-alkylbenzimidazole, (b) 2-nitrobenzyl azide to indazole.

after just 80 min of irradiation, on carrying out the reduction in the presence of CdS-(GR-Ca). This is much higher

compared to the maximum conversion rate (30%) for the same reaction under identical conditions, on using CdS-GR. Apart from CdS based nanophotocatalysts, In<sub>2</sub>S<sub>3</sub>-graphene composite was also found to be effective toward visible-light driven reduction in nitroaromatics (Yang et al., 2013). Their performance is comparable to that of the non-photocatalyst Mg-Fe hydrotalcite in reduction in nitro compounds, which gave up to 100% conversion in 2–5 h (Kumbhar et al., 2000).

Graphene-semiconductor based nanophotocatalysts also find potential applications in the reduction in carbon dioxide to organic compounds that can be used as fuels (hydrocarbons and alcohols). This strategy is particularly valuable from the environmental perspective as it assists in reducing the amount of the undesirable greenhouse gas and utilizes it to synthesize the much-needed fuels.

Graphene oxide has been coupled with ruthenium trinuclear polyazine complex photosensitizer to reduce carbon dioxide to methanol. Photosensitizers can enhance the visible light absorption by materials which otherwise possess a large band gap (Kumar et al., 2014b).

As an alternative approach, graphene has been coupled with semiconductors and these nanocomposites have been reported for photocatalytic reduction in carbon dioxide. Hydrocarbons are obtained as products on using graphene-TiO<sub>2</sub> (Liang et al., 2011), Ti<sub>0.91</sub>O<sub>2</sub>-graphene (Tu et al., 2012), TiO<sub>2</sub>-graphene 2-D sandwich hybrid (Tu et al., 2013) and graphene-WO<sub>3</sub> nanobelt composite (Wang et al., 2013). A template-based synthesis was used to prepare a hollow core-shell nanocomposite containing molecular-scale alternating titania (Ti<sub>0.91</sub>O<sub>2</sub>) nanosheets and graphene (Tu et al., 2012). The template beads of poly (methyl methacrylate) (PMMA) were later removed by microwave irradiation. The catalyst could effectively photo-reduce carbon dioxide into methane.

These graphene-based nanocomposites can also be used for selective reduction in carbon dioxide to alcohol (Hsu et al., 2013; Kumar et al., 2014a; Lv et al., 2013). For instance, graphene-modified NiO-Ta<sub>2</sub>O<sub>5</sub> was reported to be used as nanophotocatalyst to generate alcohol from carbon dioxide (Lv et al., 2013). The presence of graphene could significantly improve the performance of the catalyst in this reaction too. In the presence of NiOx loaded Ta<sub>2</sub>O<sub>5</sub>/1.0 wt.% graphene composite, the conversion rate of CO<sub>2</sub> into methanol was determined to be 0.5 mol g<sup>-1</sup> h<sup>-1</sup>, which was 3.4 times higher than the rate in the presence of the corresponding photocatalyst without graphene. It was justified that the high conductivity of graphene facilitated charge transfer and charge separation, thereby resulting in an increase in the lifetime of electron-hole pairs (analogous to mechanism 1, Fig. 3). The reactions catalyzed by graphene-semiconductor nanocomposites are summarized in Scheme 1.

## 2.2. Other modified semiconductor materials as nanophotocatalysts for organic synthesis

Though one of the most widely studied modified semiconductor nanophotocatalysts is graphene nanocomposites, nanocomposites of two semiconductors, non-metal doped semiconductors, core-shell semiconductors and metal-modified semiconductors are also proposed to be potential, convenient, eco-friendly nanophotocatalysts for organic synthesis under ambient conditions.

### 2.2.1. Nanocomposite of two semiconductors

Nanocomposites can also be prepared by combining semiconductors with desirable properties. The semiconductors are chosen based on the equivalence of their energies, which allows electron transfer to occur from one semiconductor to another. These are better photocatalysts as compared to individual semiconductors due to their tunable morphology, increased lifetime of photogenerated e<sup>-</sup>-h<sup>+</sup> pairs, greater surface area and greater absorption in the visible part of the spectrum. For example, CdS incorporated into TiO<sub>2</sub> structure (CdS-TiO<sub>2</sub> nanophotocatalyst) was used to catalyze the reduction of nitrobenzene to aniline when illuminated by UV radiation (Shrivastava, 2009). Interestingly, even the temperature maintained during sintering of the catalyst had an impact on its activity. The catalyst 10% CdS-TiO<sub>2</sub>, prepared by sintering at 500 °C showed greater activity (produced 34 μmol/dm<sup>3</sup> aniline) than catalysts with identical compositions, sintered at 300 °C (produced 4 μmol/dm<sup>3</sup> aniline) or 700 °C (produced 3 μmol/dm<sup>3</sup> aniline), when same reaction conditions were maintained. At each of the compositions studied, the optimum sintering temperature was found to be different. The sintering temperature thus markedly affected the crystallinity and morphology of the composite and hence its activity.

In another study, 1-D TiO<sub>2</sub> nanotube was coupled with CdS to improve its photoactivity for selective oxidation of alcohols (Tang et al., 2013). The catalyst combines the desirable properties of 1-D titanate nanotubes (large surface area, high pore volume, fast and long distance transport of electrons) with those of CdS (high absorbance in visible part of spectrum). In the absence of CdS, 1-D TiO<sub>2</sub> absorbs below 390 nm which corresponds to the UV region. But the presence of CdS causes absorption in the visible region. The yield for the selective oxidation of benzyl alcohol to aldehyde after 2 h with the nanocomposite (85%) was much higher than the two semiconductors in isolation (13% for CdS and 0.6% for 1-D TiO<sub>2</sub>). The irradiation caused excitation of electrons in CdS, which are then transferred to TiO<sub>2</sub>. This charge transfer takes place due to the matching of conduction band potential positions of CdS nanoparticles and titanate nanotubes, and is further augmented by their intimate contact. Thus a greater separation between excited electrons and holes is attained.

### 2.2.2. Core-shell nanocomposite

In an attempt to further enhance the interfacial contact of the semiconductor with the other component of the composite, core-shell type structures were developed. Nano core-shell composites (core@shell) comprise an inner core of a material coated with an outer shell of another material. These combine semiconductors such as CdS that can absorb in the visible part of spectrum with another semiconductor or noble metals that can act as reservoir for photogenerated electrons. Liu et al. (2012) developed a nano-core shell composite, CdS@TiO<sub>2</sub>, where both the materials are semiconductors. The material comprised of dense TiO<sub>2</sub> coating on 1-D CdS nanowires. The 1-D morphology in the CdS nanowires enhanced the electron mobility and the light absorption. This work was reported to be the first instance to have used the 1-D core-shell semiconductor composite as a photocatalyst for selective oxidation reactions. The catalyst was applied to study the conversion of benzyl alcohol and substituted benzyl alcohols to corresponding aldehydes using visible light irradiation. The

conversion rate for benzyl alcohol to benzaldehyde conversion was almost triple of that attained with 1-D CdS nanowires alone (Table 1).

The selectivity was also higher using the core@shell composite. Notably, in the presence of TiO<sub>2</sub>, CdS absorbs less in the visible region. Still, the nanocomposite gave higher yield as compared to bare TiO<sub>2</sub>. The incorporation of TiO<sub>2</sub> could increase the lifetime of photogenerated holes and electrons to a very high extent, due to the transfer of electrons from CdS to TiO<sub>2</sub> shell. This factor could effectively outweigh the detrimental effects of decrease in extent of visible light absorption that otherwise accompanied the incorporation of TiO<sub>2</sub>.

The electron spin resonance (ESR) analysis indicated that the photogenerated electrons activate molecular oxygen to form superoxide radicals (O<sub>2</sub><sup>-</sup>), which then catalyze the oxidation of alcohol. Studies revealed that photogenerated holes did not contribute much to the photocatalytic oxidation of alcohols over 1-D CdS@TiO<sub>2</sub> as these were stuck by TiO<sub>2</sub> shell.

Contrary to this, the holes also took part in selective oxidation reactions when an ultrathin TiO<sub>2</sub> layer is coated on CdS (Chen and Xu, 2013). It was reasoned that ultrathin TiO<sub>2</sub> shell augments the adsorption for alcohols and hence increases the association of the alcohols with the holes of CdS core. The ultrathin layer of TiO<sub>2</sub> in the nanocomposite also possesses the added advantage of better light absorbance and lower light reflectance, due to which enhanced excitation of electrons in CdS takes place. The ultrathin layer could not be obtained using titanium alkoxides or titanium chloride as precursors for TiO<sub>2</sub>, due to their facile hydrolysis leading to uncontrollable aggregation. To overcome this challenge, an electrostatic self-assembly of a positively charged amine functionalized CdS NSPs with negatively charged titanium(IV) bis(ammonium lactato)dihydroxide (TALH) was carried out by refluxing in aqueous medium (Fig. 7).

Instead of using a semiconductor as a reservoir for photo-generated electrons, noble metals can also be used to give noble metal@semiconductor type core-shell nanocomposites. A single core based noble metal@semiconductor nanocomposite, Pt@CeO<sub>2</sub> was prepared by introducing Pt core into a shell of CeO<sub>2</sub> (N. Zhang et al., 2011a). In the same study, the catalyst was applied for the first time to photocatalyze selective oxidation of benzyl alcohol to benzaldehyde. After 5 h of irradiation with visible light at room temperature, 37% conversion and about 98% selectivity toward benzaldehyde were reported.

Another noble metal Pd has also been investigated as the core material in CeO<sub>2</sub> shell (N. Zhang et al., 2011b). But, in this case, the resultant catalyst consisted of many cores of Pd embedded in CeO<sub>2</sub> shell. This was analogous to plum pudding model of atomic structure proposed by Thomson. The catalyst was prepared by the hydrothermal reaction of Pd colloidal solution with cerium chloride, in the presence of polyvinylpyrrolidone (PVP) as the capping agent to prevent the self-aggregation of Pd nanoparticles. The catalyst was also studied for selective oxidation reaction of alcohols to carbonyls. The reaction mixtures were irradiated ( $\lambda > 420$  nm) at room temperature and ambient pressure for 20 h. The multi core@shell catalyst was reported to give a higher yield (28%) and greater selectivity (100%) compared to Pd supported on CeO<sub>2</sub> (yield – 5% and selectivity – 71%). The multi-cored structured catalyst was more effective due to its greater surface area, better metal-CeO<sub>2</sub> interfacial contact, greater charge

transfer, better adsorption of benzyl alcohol and greater ease of desorption of benzaldehyde.

The core-shell nanocomposites can also be used as co-catalysts. For example, the presence of Ni@NiO core-shell increased the photoactivity of doped InTaO<sub>4</sub>, under visible light irradiation (Tsai et al., 2011). The catalyst was demonstrated to be effective in the CO<sub>2</sub> reduction to methanol. The core@shell co-catalytic nanoparticles receive electrons from the catalyst (doped InTaO<sub>4</sub>) and then interact with the carbon source.

### 2.2.3. Non-metal doped semiconductor material

A semiconductor may be doped with a metal or a non-metal to enhance its photocatalytic activity (Kumar and Devi, 2011; Naik et al., 2014). The non-metal dopant increases the photoactivity of the semiconductor in the visible part of spectrum by enhancing the surface area and diminishing the band gap of semiconductor. For example, band gap of TiO<sub>2</sub> reduced from 3.02 eV to 2.85 eV on doping with nitrogen. Thus, the N-TiO<sub>2</sub> catalyst prepared absorbed in the visible region and was yellow-colored (Wang et al., 2009). Also, doping gives rise to new impurity energy levels, causing absorption in the visible part of spectrum. In addition, lower recombination rate of photogenerated holes and electrons was indicated by the photoluminescence spectra. For instance, X-ray photoelectron spectroscopy studies of N-doped semiconductors (N-TiO<sub>2</sub>) indicated that the anionic nitrogen was incorporated in the lattice in the form of O-Ti-N linkages (Selvam and Swaminathan, 2012). The incorporation of nitrogen in the TiO<sub>2</sub> lattice reduces oxygen vacancies, thereby decreasing the e<sup>-</sup>-h<sup>+</sup> recombination rate.

N-doped TiO<sub>2</sub> (anatase) was studied for the reduction in substituted aromatic nitro compounds to corresponding amines (Wang et al., 2009). Contrary to oxidation reactions, reduction reactions are usually done in the presence of NaI or KI. The I<sup>-</sup> ions act as scavengers for the holes. The catalyst was synthesized by a modified sol-gel process using urea as the precursor for nitrogen. The selective reduction reaction was carried out in the presence of methanol using the N-TiO<sub>2</sub> nanophotocatalyst. Excellent yields (>90%) of corresponding amines were obtained in a very short reaction time (<20 min). The catalyst was quite tolerant to other functional groups such as carbonyl, halogen, amino, hydroxyl and carboxylic acid groups.

Another technique to prepare N-doped TiO<sub>2</sub> is simple wet impregnation method using nano titania and hydrazine hydrate as precursors for nitrogen (Selvam et al., 2012). The nano N-TiO<sub>2</sub> so prepared catalyzed the reductive cleavage of azoxybenzene. The obtained product was found to depend on the solvent. In neat methanol, the product was aniline, whereas in aqueous methanol (80% methanol–20% water), corresponding 2-phenyl indazoles were formed (Scheme 2). This was assigned to different mechanisms being followed in different solvents. The yield was higher in both cases, as compared to the use of pure TiO<sub>2</sub>, when reaction was studied at room temperature in an atmosphere of nitrogen.

In another report, nano N-doped TiO<sub>2</sub> was used in one-pot synthesis of quinaldines from nitrobenzene. The reaction was carried in ethanol using irradiation with UV and visible light (Selvam and Swaminathan, 2012). Quinaldines are generally used in anti-malarial drugs (Fig. 8).

The effect of catalysts toward this reaction was reported to decrease in the order N-TiO<sub>2</sub>, Pt-TiO<sub>2</sub>, Au-TiO<sub>2</sub>, Ag-TiO<sub>2</sub> and bare TiO<sub>2</sub>. Thus it can be inferred that for this reaction doping of semiconductor with non-metal enhanced the activity more than the doping by a metal. But the trend and the inference cannot be generalized for all reactions due to limited evidence in this regard.

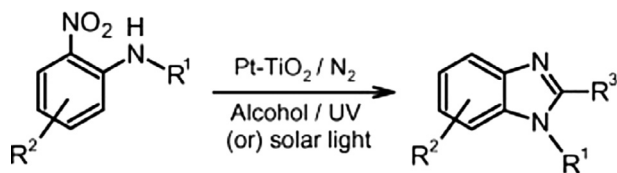
#### 2.2.4. Metal-modified semiconductor

Another alternative to widen the scope of photocatalyzed organic reactions by semiconductors is to introduce metals or metal complexes as co-catalysts or as reaction sites. The mechanism, by which these metal-modified semiconductors influence the photocatalytic activity of semiconductors, as conceived, is different from that of non-metal doped ones. These metals or metal complexes co-catalysts act as mediators between the reactants and the semiconductors. The semiconductor undergoes excitation on absorbing radiation. The excited electrons from semiconductors migrate to energy levels in the co-catalyst and activate it. The activated co-catalyst then provides active sites for the reaction to occur. Thus the metal or metal complex nanoparticles contribute in increasing the lifetime of the photogenerated e<sup>-</sup>-h<sup>+</sup> pairs.

J. Li et al. (2011) reported that iridium complexes coupled with CdS nanoparticles catalyze hydrogenation of alkenes and carbonyls when irradiated with visible light. Here, it is worth emphasizing that when instead of iridium complexes, nanoparticles of elemental iridium were loaded on CdS, and no activity for photoreduction of cyclohexanone was observed. Only the iridium complexes could successfully use the harvested light energy to drive the reaction.

Apart from the yield, the metal or the metal complex introduced as co-catalyst affects the chemo selectivity of the reaction. This is evident from a recent research done by Kominami et al. (2014). In this work, comparative observations were done in the deoxygenation of epoxides in alcoholic suspensions, when photocatalyzed by metal nanoparticles loaded on TiO<sub>2</sub>. Ag nanoparticles loaded on TiO<sub>2</sub> could direct the selective reduction of (2,3-Epoxypropyl) benzene epoxide to allylbenzene along with the selective oxidation of 2-propanol to acetone. After 90 min of irradiation with UV light at room temperature, 99% yield of allylbenzene was obtained, without the use of any reducing agent. Instead, when gold or copper was used as co-catalyst, production of hydrogen gas was a prominent reaction.

The metal-doped semiconductor catalyst can also act as micro-heterogeneous centers, and catalyze simultaneous oxidation of one substrate and the reduction in the other. For instance, the metal (Ag or Pt) doped nano-TiO<sub>2</sub> has been proposed to be a productive catalyst for the simultaneous oxidation and reduction followed by condensation reactions. The catalyst could convert aromatic azides to *N*-heterocyclics



**Scheme 4** Conversion of *N*-substituted 2-nitroanilines to disubstituted benzimidazoles (Selvam and Swaminathan, 2011).

(2-alkylbenzimidazoles and indazole) in O<sub>2</sub>-free alcoholic suspensions. Moreover, the catalyst was determined to be effective not only under UV illumination, but also under solar radiation (Selvam et al., 2009). Nano-photocatalysts catalyzed the various possible steps of the overall reaction-oxidation of alcohol, reduction in nitroaromatic and cyclization. The exact steps that take place were different in case of different substrates, giving rise to different products. In case of 2-nitrophenyl azide, 2-alkylbenzimidazole was obtained as the main product. On the other hand, when 2-nitrobenzyl azide was used as the substrate, the product was indazole (Scheme 3). Both imidazoles and indazoles are well known for their wide range of biological activities. The BET surface area indicated a slight reduction in the surface area for the doped catalyst relative to bare nano-TiO<sub>2</sub>. In spite of this, the yield of the product was more with doped catalyst. Thus, the positive effect of increased lifetime of e<sup>-</sup>-h<sup>+</sup> pairs in the presence of the metal seems to overcome the surface area effects.

Pt-TiO<sub>2</sub> prepared by photodeposition was also reported to be an effective catalyst for the synthesis of disubstituted benzimidazoles from *N*-substituted 2-nitroanilines or 1,2-diamines under UV and solar light in different alcohols (Selvam and Swaminathan, 2011) (Scheme 4). Another photocatalytic transformation that combined redox reaction and cyclization is the synthesis of quinaldines from anilines using Au-loaded TiO<sub>2</sub> under UV irradiation (Selvam and Swaminathan, 2010). The reaction was carried out in ethanol.

In another work, for the first time, both small and large Au nanoparticles were loaded on TiO<sub>2</sub>, and the resulting catalyst was used for reductive *N*-alkylation of aniline and nitrobenzene (Stibal et al., 2013). The differently sized nanoparticles act as reaction centers for different elementary reactions of the overall reaction. The catalyst comprised of both relatively large (5–13 nm: 60%) and small (< 4 nm: 40%) Au nanoparticles. The semiconductor on irradiation produced photogenerated e<sup>-</sup>-h<sup>+</sup> pairs. The photogenerated holes on semiconductor oxidized alcohol to aldehyde (Fig. 9). The aldehyde then condensed with aniline to give an imine. The photogenerated electrons were transferred to the larger Au nanoparticles. The smaller Au nanoparticles were not effective sinks due to their lower metallic character. The electrons on larger nanoparticles reduced protons released by oxidation of alcohol, into hydrogen. The hydrogen so produced got adsorbed on the smaller nanoparticles preferentially due to their greater surface area. Thus, this time, the smaller Au nanoparticles acted as the active sites to hydrogenate imines to *N*-alkylated products. In the absence of these smaller nanoparticles, imines would have been the major product. On carrying out the reaction with aniline and various terminal alcohols, using four 16 W UV-A lamps (approx. 350 nm source), up to 100% conversion rates were obtained after 4 h, either the monoalkylated or dialkylated moiety being the major product depending on the alcohol.

The catalyst was also proposed for the photo-cyclization of 5-aminopentanol to lactam. The yield of  $\delta$ -valerolactam after 4 h of irradiation was 16.3%. The catalyst was stable as no metal leaching was deduced using Atomic Absorption Spectroscopy after the reaction. The presence of electron releasing groups and electron withdrawing groups influenced the reactivity as dictated by conventional inductive and resonance effects.

The metal doped semiconductors are also more efficient catalysts for photoreduction of carbon dioxide. Pt-TiO<sub>2</sub>

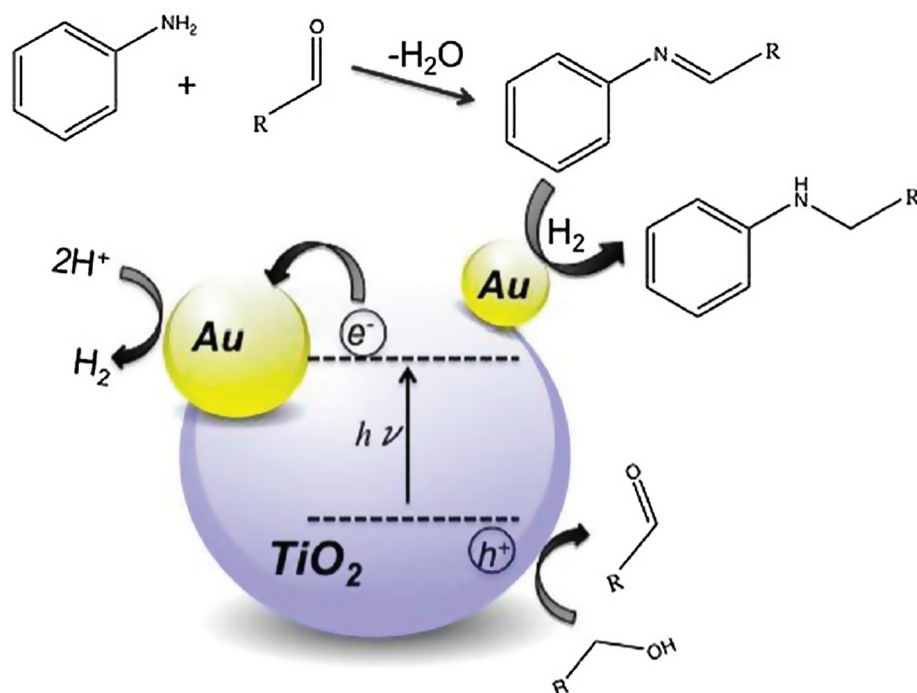


**Figure 9** Mechanism of reductive N-alkylation of aniline and nitrobenzene using terminal alcohols with Au nanoparticles loaded on  $\text{TiO}_2$  (Stibal et al., 2013).

nanotubes (Feng et al., 2011), Pt- $\text{TiO}_2$  nanorods (Ohno et al., 2014), nanocrystalline nickel loaded  $\text{TiO}_2$  (Ola and Maroto-Valer, 2011) and nitrogen and nickel co-doped nano-titania (N-Ni- $\text{TiO}_2$ ) (Fan et al., 2011) are found to be effective photocatalysts for reducing carbon dioxide to various hydrocarbons and derivatives.

In order to further reduce  $e^-$ - $h^+$  recombination rate, Roy et al. in 2013 modified the metal-semiconductor nanocomposite by introducing graphene into it (Roy et al., 2013). The catalyst prepared was semiconductor-based ternary nanocomposite, G-ZnO-Au. It was based on the view that it is energetically more favorable to transfer photogenerated electrons from conduction band of semiconductor to graphene and then to the Fermi energy level of Au nanoparticles, rather than the direct semiconductor to Au electron transfer. Hence, the presence of graphene facilitates faster transfer of electrons from the semiconductor to Au nanoparticles, which lengthen the lifetime of  $e^-$ - $h^+$  pairs. Upon ultraviolet light irradiation ( $\lambda < 420$  nm), G-ZnO-Au nanocomposite in methanol gave a yield of 97.8% aniline after 140 min. This was 3.5 and 4.5 times higher than the yields produced by commercial  $\text{TiO}_2$  and ZnO nanospheres respectively. The role of methanol was to trap the holes produced. Also, for the first time, the intermediates (nitrosobenzene and phenylhydroxylamine) in the reduction in nitrobenzene to aniline were detected by surface assisted laser desorption/ionization mass spectrometry.

In a combinational strategy, catalysts have been fabricated by co-doping semi-conductors with both metals and non-metals. Though the catalysts so synthesized have been chiefly considered for degradation of organic compounds and dyes, their utility can be extended in future to organic synthesis as well.  $\text{TiO}_2$  was doped both with a metal (lanthanum) and with a non-metal (nitrogen) (Li et al., 2015). The catalyst so synthesized, La-N- $\text{TiO}_2$ , demonstrated enhanced visible light

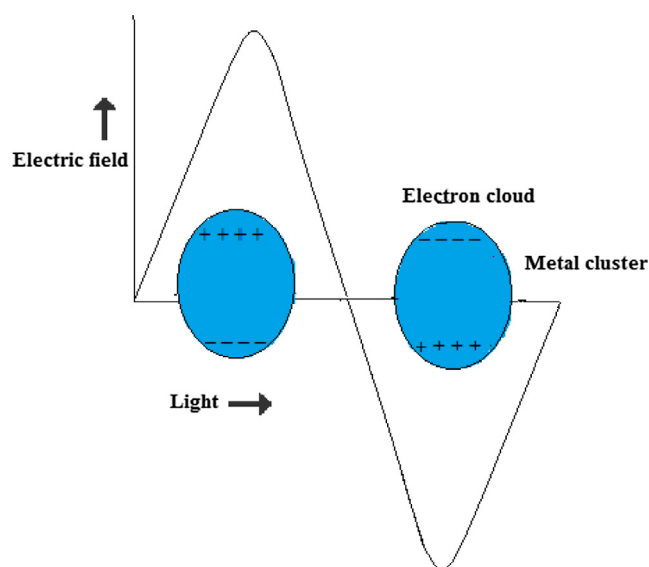


**Figure 10** SPR showing oscillations of electrons when stimulated by electromagnetic waves.

absorption and photocatalytic activity in degradation of phenol. In another study, nano-sized  $\text{TiO}_2$  was co-doped with both cobalt and sulfur and was found to be efficient in degradation of phenol and dyes (Siddiqi et al., 2015). In both these studies, catalysts were prepared by sol-gel method. Microwave-assisted hydrothermal synthesis has also been used to synthesize co-doped semiconductors, as in the synthesis of neodymium-nitrogen-phosphorus tri-doped (Jiang et al., 2015) and samarium, nitrogen and phosphorus tri-doped (Wang et al., 2015)  $\text{TiO}_2$ .

Also, very recently, TiO<sub>2</sub>/maghemite-silica nanocomposite as a photocatalyst has been reported (Colmenares et al., 2016). The main merit of this photocatalyst was its easy recoverability through magnetic separation. It could photo-oxidize benzyl alcohol (50% conversion) with high selectivity toward benzaldehyde (90% selectivity).

Quite different from studies on composite materials, Eskandari et al. (2014) reported that nanostructures of CdS were efficient in bringing about reduction in nitro compounds to corresponding amines. In the presence of this catalyst and ammonium formate as hole scavenger, 100% conversion of nitrobenzene could be achieved after 20 h of irradiation with blue LED.

### 3. Surface Plasmon Resonance-mediated nanophotocatalyst

Apart from semiconductors, nanoparticles of metals can also act as efficient photocatalysts under visible light irradiation. In such cases, unlike the role of metal as a co-catalyst (as discussed in Section 2.2.4), the metal nanoparticles themselves absorb UV/visible radiation to catalyze a reaction. Most commonly, the nanoparticles of noble metals (e.g. silver and gold) are studied, as these can absorb both UV and visible radiations.

But the absorption mechanism by metals is different in the UV and visible regions of the spectrum. The absorption in UV region by nanoparticles is because of inter-band transition. Instead, absorption in the visible part of the spectrum is due to Surface Plasmon Resonance (SPR) Effect. SPR is the collective oscillations of electrons on the surface of a solid or liquid. This is the result of stimulation caused when an electromagnetic radiation is incident on the material (Mie, 1908). Surface electrons oscillate against the restoring force of the positive nuclei with certain frequency. Resonance condition occurs when this frequency equals the frequency of incident radiation and Surface Plasmon Resonance (SPR) results. When the SPR is in materials of nanoscale dimensions, it is of practical importance and is called Localized Surface Plasmon Resonance (LSPR) (Fig. 10).

The LSPR frequency depends on the metal, the shape and size of the nanoparticle, and also on the dielectric properties of the surrounding medium (Moore and Goettmann, 2006). Noble metals and their alloys can be very good photocatalysts due to LSPR effect. In the case of metals such as silver and gold, the LSPR resonance energy is in visible region of spectrum, making them suitable photocatalysts to harness the visible spectrum of sunlight. LSPR excitation in these noble metals builds up high photon intensity (strong electric fields) and a large population of energetic electrons at nanostructured surfaces. In their review, Park et al. (2014) have pointed out that plasmon excitation can also generate energetic electrons (termed as 'hot electrons') that are not in thermal equilibrium with the atoms of noble metal and can be instrumental in bringing about chemical transformations.

#### 3.1. Mechanism of photocatalytic activity for the organic synthesis by LSPR

An analysis of the suggested mechanism of action of surface plasmons (Kochuveedu et al., 2012; Linic et al., 2013) indicates two possibilities:

- i. Indirect photocatalysis: In this case, photon energy produced by excitation of LSPR is transferred to a nearby semi-conductor through plasmon-induced resonant energy transfer (PIRET) or direct electron transfer (DET) (Li et al., 2013). The chemical transformations are then effected by the photogenerated electrons and holes of the semiconductor.
- ii. Direct photocatalysis: In this case, excitation of LSPR causes chemical transformations of adsorbates on the surface of the metal nanoparticles itself. For instance, Ag nanoparticles supported on  $\alpha$ -Al<sub>2</sub>O<sub>3</sub> particles were studied for commercially important reactions such as epoxidation of ethylene under visible light irradiation (Christopher et al., 2011). From DFT studies, it was inferred that the Ag nanoparticles got stimulated by LSPR effect and transferred electrons to the antibonding orbitals of oxygen molecule. This facilitates the rate-limiting O<sub>2</sub>-dissociation reaction. The cubic nanostructures were determined to be more effective photocatalysts than nanospheres and nanowires because of their better selectivity (Christopher and Linic, 2008, 2010) and higher plasmon intensities (Christopher et al., 2010).

Apart from the shape of nanoparticles, the efficiency and selectivity of the LSPR-mediated photoactivity also depend on factors such as size of the nanoparticles, wavelength and intensity of the radiation, method of preparation, loading percentage of metal and reaction temperature.

In some cases, a combination of direct and indirect photocatalysis takes place, whereby both the semiconductor and the metal nanoparticles activate the reactants.

#### 3.2. Preparation of surface plasmon mediated photocatalyst

The various methods to prepare nanoplasmonics are deposition-precipitation, photoreduction or photodeposition, ion exchange and encapsulation. The deposition-precipitation method involves the immersion of the support material and the precipitating agent in an aqueous solution of the precursor compound of the metal. This is followed by washing the product and heating in air or an atmosphere of H<sub>2</sub> at a temperature of 200–400 °C to reduce the metal ion to metal. The loading amount and the size of the metal nanoparticles depend on the calcination temperature and the pH of reaction mixture. The method is particularly advantageous for attaining narrow size distribution of small size noble metal nanoparticles, usually less than 5 nm, on a support (Zhou et al., 2012).

Photoreduction is used to deposit noble metal nanoparticles on a semiconductor support using light irradiation. The metal precursor is dispersed and allowed to be adsorbed on the semiconductor support. On light irradiation, electrons in the semiconductor get excited from valence band to the conduction band. These excited electrons then reduce the metal ion of the metal precursor. A suitable hole scavenger is added to prevent the accumulation of holes. High deposition ratio can be attained and aggregation is effectively avoided as the method does not require any further calcination. But, the reproducibility is difficult, even though there is an inverse relation between the particle size and wavelength of irradiation. Along these lines, colloidal Au nanoparticles were loaded on TiO<sub>2</sub>, by irradiating a suspension of TiO<sub>2</sub> powder and tetrachloroauric acid

(HAuCl<sub>4</sub>) at  $\lambda > 300$  nm at 298 K. The loading required the use of oxalic acid as hole quencher (Tanaka et al., 2012).

Another method, ion exchange can be used when the solubility of obtained products is lower than that of reactants (Zhou et al., 2012). Even though the condition imposed limits the applicability of the method, yet it is useful as a uniform distribution of nanoparticles can be attained. The ion exchange step is followed by calcination or photoreduction. A combination of deposition-precipitation and ion-exchange method was used to develop the photocatalyst AgI/AgCl/H<sub>2</sub>WO<sub>4</sub> (C. Liu et al., 2014). First, AgCl/H<sub>2</sub>WO<sub>4</sub> substrate was prepared via a deposition-precipitation method by dispersing AgNO<sub>3</sub> and KCl, at room temperature in the presence of H<sub>2</sub>WO<sub>4</sub>. Following this, a stoichiometric amount of KI solution was added into the AgCl/H<sub>2</sub>WO<sub>4</sub> dispersed in deionized water and stirred magnetically for 20 min. The ion exchange of AgCl with KI resulted in the double heterojunction composite AgI/AgCl/H<sub>2</sub>WO<sub>4</sub>. The ratio of AgI to initial AgCl can be varied by changing the concentration of KI.

In encapsulation strategy, noble metals are embedded in a shell of another compound, to give structures denoted by core@shell. The use of inert materials such as SiO<sub>2</sub> as the shell, protects the active metals from oxidation, increases their stability and prevents their agglomeration (Zhou et al., 2012). This core@shell structure is then embedded in a photocatalyst matrix, like a semiconductor. The encapsulation in a shell modifies the optical properties of the metal nanoparticles. For example, Ag@Cu<sub>2</sub>O core-shell nanoparticles showed a red shift in the LSPR band with enhancement in the Cu<sub>2</sub>O shell thickness. The average diameter of Ag core was determined to be approximately 30 nm. After encapsulation, the total diameter of the core@shell increased to 100 nm (Li et al., 2013).

Other methods such as micro-emulsion based bottom-up self-assembly (G. Wang et al., 2012), solvothermal (Shi et al., 2014) and sputtering (Avasthi et al., 2010) are also used to synthesize nanoplasmonics. In a unique innovative strategy, sugarcane juice has been used to prepare silver supported on silver chloride (Ag@AgCl photocatalyst) (Kulkarni and Bhanage, 2014). It involves the reaction of AgNO<sub>3</sub> with sugarcane juice at 80 °C for 20 min. The sugarcane juice was used as a single source of reducing agent (glucose component), organic capping agent (components such as oxalic acid, malic acid, citric acid, succinic acid and D-gluconic acid) and chloride ions. The catalyst obtained had stable particles of uniform shape and size (less than 50 nm). The photocatalyst has been found to be effective for degradation of methylene blue and methyl orange. This catalyst can in future be investigated for various photoredox reactions in organic synthesis.

### 3.3. Selective organic transformations photocatalyzed by surface plasmon mediated catalyst

#### 3.3.1. Selective oxidation reactions

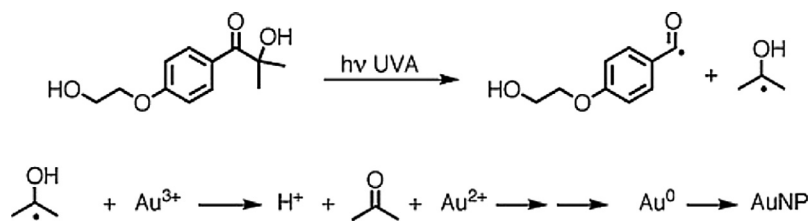
Imine is an important class of organic compounds used in the synthesis of other organic compounds such as tetrahydropyridine, oxaziridine and quinolone. Generally, imine/imine derivatives are either prepared by the condensation of an amine with a carbonyl compound or by oxidation of amines. Various catalysts such as rhodium complexes, noble metals such as gold powder, noble metals supported on Al<sub>2</sub>O<sub>3</sub> or

TiO<sub>2</sub> or gold-palladium supported nanoparticles on porous steel fiber are considered to convert amines to imines. These require high temperature and high pressure conditions (Chen, 2013; Grirrane et al., 2009; H. Guo et al., 2011; Zhu et al., 2008). In an attempt to carry the benzylamine to imine oxidation under milder conditions, photocatalyst with Au-Pd alloy loaded on ZrO<sub>2</sub> (Au-Pd/ZrO<sub>2</sub>) was studied (Chen, 2013). TEM studies of the catalyst revealed nanoparticles with size in the range of 1–10 nm, with 60% of the particles having particle size 4–5 nm. The yield of imine obtained is much higher than the obtained yield when the reaction is carried out thermally under identical conditions, but without light illumination. Maximum yield was obtained when the alloy Au-Pd was used in the composition ratio 1:1.86 (Au:Pd). The alloy enhanced the charge heterogeneity and thus the affinity for the reactants. The reaction rate also increased with an increase in the intensity of irradiation and temperature. Though the reaction takes place photochemically, heating to a higher temperature gave higher yields.

Silver compounds such as Ag<sub>2</sub>O and AgI are unstable with respect to photolytic decomposition of Ag, but are self-stabilized after partial decomposition (X. Wang et al., 2011; Yu et al., 2012). Based on this concept, a novel photocatalyst was prepared by loading AgI nanoparticles on titanate nanotubes (TNTs) (Zheng et al., 2014). AgI partially decomposed to give Ag/AgI nanoparticles supported on titanate. On carrying out the conversion of benzylamine to imine in the presence of this catalyst under visible light illumination, high conversion rates (45–90%, depending on the AgI amount in the sample) and high selectivity were obtained (>94%). It is an encouraging result toward the development of photocatalysts as reaction proceeded under milder conditions (400 °C and 1 atm O<sub>2</sub> pressure) compared to thermal reactions. The activity of catalyst was attributed to LSPR and not to the semiconductor mechanism. This is proved by the observation that the catalytic activity was retained even at wavelength >443 nm, much greater than the wavelength that corresponds to the band gap in AgI (2.8 eV). The proposed LSPR mechanism was further proved by the fact that the activity of the catalyst increased with an increase in temperature, which is a specific metal characterization. Thus the mechanism involves LSPR absorption of visible radiation by Ag particles followed by the transfer of electrons to the conduction band of AgI. Resulting positively charged silver nanoparticles then oxidize benzylamine to benzaldehyde. This was followed by the condensation of benzaldehyde and the remaining benzylamine to give the imine product.

Selective oxidation reaction of benzyl alcohol to benzaldehyde is another industrially important reaction. Bimetallic AuPd nanowheel-like heterostructures could bring about 97.7% conversion of benzyl alcohol, with 98% selectivity toward benzaldehyde, under xenon-lamp irradiation within 6 h (Huang et al., 2013).

Supported plasmonics have also been widely studied for this reaction. Au/CeO<sub>2</sub> catalyst prepared by photochemical decomposition gave almost 100% conversions with high selectivity (99%) toward benzaldehyde in 20 h of reaction time, under green light illumination (Tanaka et al., 2011). Gold nanoparticles over supports such as hydrotalcite (HT),  $\gamma$ -Al<sub>2</sub>O<sub>3</sub> and ZnO were prepared by solvent-less dry photochemical method and were determined to be good catalysts for oxidation of benzyl alcohol to benzaldehyde (Tapley



**Scheme 5** Generation of Au nanoparticle *via* Norrish type I photocleavage of the I-2959 ketyl radical precursor (Tapley et al., 2011).

et al., 2011, 2013). The preparation involved the reduction of  $\text{HAuCl}_4$  by ketyl radicals generated from a photoinitiator benzoin I-2959, in the presence of a solvent  $\text{CH}_3\text{CN}$ , when irradiated with 5 UVA lamps of intensity  $65 \text{ W/m}^2$  (Scheme 5).

This technique was a distinct advantage over the chemical reduction method as it did not involve the use of large amounts of water and the catalyst could be easily recovered. The supported Au nanoparticles prepared by this method, did not show any agglomeration following the LSPR, which was the case in colloidal Au nanoparticles.

Laser ablation is another method for the preparation of nanoparticles of gold on supports such as HT and metal oxides (Alejo et al., 2012; Tapley et al., 2013). In the work by Alejo et al. (2012), polymorphic gold nanoparticles were subjected to a laser of wavelength 532 nm at an intensity of  $0.66 \text{ J/cm}^2$ . The spherical gold nanoparticles had lower size (4 nm) and lower polydispersity compared to the ones prepared by dry photochemical method. The catalysts prepared by the two different methods were compared for their activity toward oxidation of sec-phenylethylalcohol and benzylalcohol, using  $\text{H}_2\text{O}_2$  as initiator,  $\text{CH}_3\text{CN}$  as solvent, under illumination of a 530 nm (Tapley et al., 2013). The larger particles obtained by dry photochemical method were found to be slightly better catalysts in most cases than the smaller nanoparticles obtained by laser ablation technique. Surprisingly, this violates the expected surface area effects. The reason is not clearly known, but may be due to better light absorption by larger nanoparticles. The retention of activity for gold supported on HT was much greater for the catalyst prepared by dry photochemical method than the one prepared by laser ablation. The support used also affects the efficiency and reusability of the catalyst. HT was a good support for the Au nanoparticles as the high basicity of HT favors a great interaction with the alcohol, promoting its oxidation.

Au nanoparticles supported on zeolites combine the advantages of strong visible light absorption by Au nanoparticles with the high tendency of zeolites to adsorb reactants. Zeolites are good adsorbents and can adsorb reactants through hydrogen bonds or acid-base interactions. Zhang et al. in 2012 developed gold nanoparticles supported on zeolite for selective photooxidation of aromatic alcohols. The reaction was studied under visible light irradiation (X. Zhang et al., 2012). High selectivity (99%) for the formation of benzaldehyde was obtained at  $40^\circ\text{C}$ . In addition to the particle size and surface area of the catalyst, the photoactivity also increased with an increase in the polarity of the reactant (4-methylbenzylalcohol < 2-phenyl ethanol < benzyl alcohol < 4-methoxybenzy alcohol < cinnamyl alcohol). This is because of greater interaction of the polar molecule with the electromagnetic fields generated by LSPR effect of Au nanoparticles. The type of zeolite support also affected the

extent of adsorption of reactant and hence the photocatalytic ability. The mechanism was a direct photolysis type, where the excited gold nanoparticles activate molecular oxygen to form  $\text{O}_2^-$  species, and abstract  $\alpha\text{-H}$  from methylene group of benzyl alcohol causing its selective oxidation to benzaldehyde.

Au nanoparticles supported on  $\text{TiO}_2$  are also used for oxidation of cinnamyl alcohol. The products were cinnamaldehyde (with 90% selectivity) and cinnamic acid (with 10% selectivity) (Naya et al., 2010). The obtained conversion rate after 8 h irradiation was 8%. On the other hand, UV irradiation resulted in degradation of cinnamyl alcohol, further proving the difference in mechanism of action under visible and UV irradiation, as discussed previously (Section 3). Ag based nanophotocatalyst obtained by anchoring the dye  $[\text{Ru}(\text{bpy})_3]^{2+}$  (bpy = 2,2'-bipyridine) on the surface of core-shell  $\text{Ag@SiO}_2$  nanomaterial effectively oxidized styrene and styrene derivatives in the presence of  $\text{O}_2$  at room temperature (Mori et al., 2010).

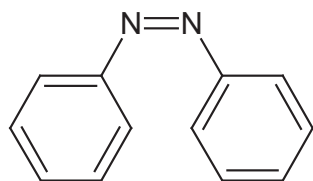
Au nanorods were introduced as antennas on  $\text{TiO}_2$  in order to extend the harvesting of light energy to near infra-red region (L. Liu et al., 2013). The introduction of Au nanorods could enhance the activity by 2.8 times in the oxidation of 2-propanol to acetone. In another study, the introduction of Pt as co-catalyst to Au/ $\text{TiO}_2$  system could further enhance the activity (5–9 times greater than that of Au/ $\text{TiO}_2$ ) in the same reaction (Tanaka et al., 2013).

### 3.3.2. Selective reduction reactions

The excited electrons generated due to LSPR effect of metal nanoparticles can be employed to carry out reduction reactions. The reduction in reactions with more negative reduction potentials requires the presence of more energetic electrons. The ability of different catalytic systems obtained by supporting gold on different supports such as  $\text{CeO}_2$ ,  $\text{TiO}_2$ ,  $\text{ZrO}_2$ ,  $\text{Al}_2\text{O}_3$  and zeolite Y, to reduce nitro-aromatics to azo compounds, hydrogenate azobenzene to hydroazobenzene, reduce ketones to alcohols, and deoxygenate epoxides to alkenes was studied (Ke et al., 2012, 2013). It was revealed that even though the supports for the metal nanoparticles generally do not absorb in the visible part of spectrum and are not directly involved, they affect the catalytic activity by determining the particle size of nanoparticles and the extent of adsorption of reactants. In particular, Au/ $\text{CeO}_2$  was found to be most efficient photocatalyst in these studies. This was suggested due to the strong interface action of Au and  $\text{CeO}_2$ , which resulted in greater light absorption by Au/ $\text{CeO}_2$  system. The gold nanoparticles absorb visible light due to LSPR effect. These high energy plasmon electrons then abstract hydrogen from the solvent (e.g. isopropanol) forming Au-H species. The hydrogen is then transferred to the reactant molecule having

**Table 2** Photoactivity of Au/CeO<sub>2</sub> for reduction reactions under simulated sunlight (Ke et al., 2013).

Reactions	Time (h)	Temperature (°C)	Conversion (%)	Selectivity (%)
Reduction in nitrobenzene	3	40	66	95
Hydrogenation of azobenzene	6	30	33	79
Reduction in acetophenone	24	40	31	94
Deoxygenation of styrene oxide	20	30	18	89

**Figure 11** Structure of cis-azobenzene.

double bonds (N=O, C=O, N=N or epoxide bond) leading to reduction. These catalysts were also found to be quite effective for reduction reactions when stimulated by sunlight (Table 2).

These plasmonic nanophotocatalysts are also studied for the reduction in carbon dioxide to hydrocarbons. The incorporation of Ag nanoparticles on AgX halides (X: Cl or Br) considerably increased the photoactivity of pristine AgX due to the LSPR effect of Ag nanoparticles (An et al., 2012). Another nanophotocatalyst for the reduction in carbon dioxide to methanol was prepared by loading Ag nanoparticles on TiO<sub>2</sub> catalyst (Ag/TiO<sub>2</sub>). Under UV/visible irradiation, the mechanism involved a synergistic effect of LSPR of Ag nanoparticles and the valence-conduction band excitation of electrons of the semiconductor (E. Liu et al., 2014). The yields of methanol obtained with Ag/TiO<sub>2</sub> photocatalyst were higher than those obtained with bare TiO<sub>2</sub> under UV or UV-visible regions of spectrum. Also, unlike bare TiO<sub>2</sub>, the composite was quite effective to photocatalyze the reaction, even under visible light. It was also noted that after 3 h of irradiation, using Ag/TiO<sub>2</sub>, the methanol yield (405.2 mol/g-cat) obtained under UV-visible light irradiation is almost double than the sum of methanol yield (220.0 μmol/g-cat) when UV and visible light irradiations are used separately. These data strongly indicate a synergistic effect between the band-gap excitation of electrons in the semiconductor and the LSPR mechanism of the silver nanoparticles under UV-visible irradiation. The electrons excited by UV in TiO<sub>2</sub> are transferred to Ag nanoparticles. The energy of trapped electrons on Ag nanoparticles is further increased by the LSPR effect. This increases the lifetime of photogenerated e<sup>-</sup>-h<sup>+</sup> pairs. Yet, the optimum loading for the catalyst was 2.5% Ag/TiO<sub>2</sub>, beyond which an increase in the percentage of silver nanoparticles reduced the activity of the catalyst. It may be because beyond the optimum amount, Ag nanoparticles may operate as recombination centers for e<sup>-</sup>-h<sup>+</sup> pairs.

Not only TiO<sub>2</sub>, but other supports such as HT and Al<sub>2</sub>O<sub>3</sub> were also considered for loading metal nanoparticles. Au nanoparticles were loaded on the support ZrO<sub>2</sub> and the resulting catalyst photocatalyzed the reduction in nitrobenzene to azobenzene (Fig. 11) (H. Zhu et al., 2010).

The product azobenzene cannot be obtained thermally by the reduction in nitrobenzene as it is unstable with respect to dissociation to aniline. This shows that photocatalysts not only have the potential of providing alternate routes to thermal reactions, but can also open new up synthetic gateways. The activity of the catalyst got affected by the average size and the polydispersity of the nanoparticles, which in turn depend on the metal loading, the pH at which the loading is done and the support used (Tapley et al., 2011; Lin et al., 2013).

### 3.3.3. Addition reaction

Catalyst obtained by supporting Au nanoparticles on N-doped TiO<sub>2</sub> was studied for catalyzing hydroamination of alkynes to yield imines (Zhao et al., 2013). N-doped TiO<sub>2</sub> interacts more strongly with the reactants and hence was chosen as the support instead of bare TiO<sub>2</sub>. The highest yield was obtained for the reaction of aniline with 4-phenyl-1-butyne (90%). The selectivity for the desired imine product was 91%. The reaction sample was irradiated for 25 h at 40 °C. But, it was observed that the catalyst got deactivated in the presence of highly basic reactant such as aliphatic aminohexane. Non-terminal alkynes also gave lower yields due to steric factors. Mechanism proposed involved a transfer of LSPR generated electrons from the metal to the semiconductor. This leaves Au nanoparticles positively charged, which then activate the nucleophilic amine. In turn, the Ti<sup>3+</sup> sites on the electron-rich semiconductor activate the alkynes.

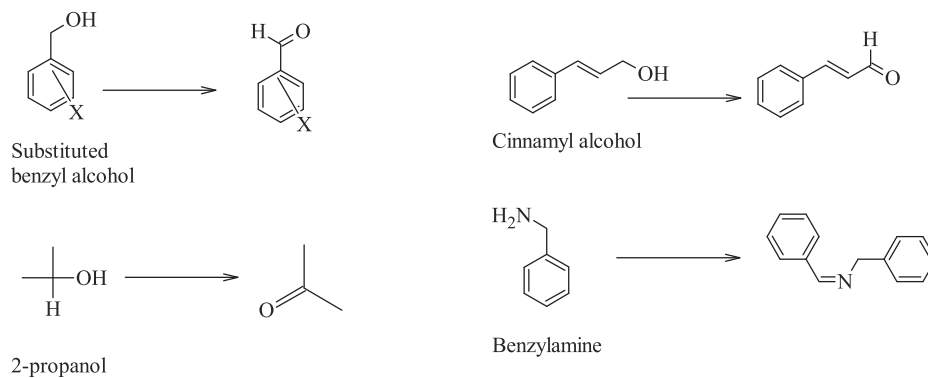
Scheme 6 illustrates the selective organic transformations photo-catalyzed by plasmonics.

## 4. Metal-organic charge-transfer based nanophotocatalyst: MOF

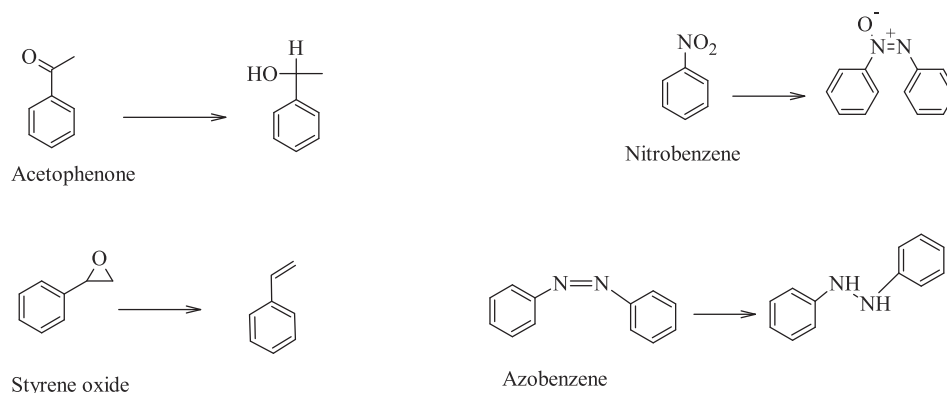
Exploration of Metal-Organic Frameworks (MOFs) as photocatalytic materials is a newer field of research, as compared to studies on semiconductors and plasmonics. MOF is a class of porous crystalline materials comprising of metal ions linked together by organic bridging ligands. The different methods to prepare MOF are solvothermal synthesis (Pachfule et al., 2011), slow evaporation synthesis (Du et al., 2006), microwave assisted synthesis (Klinowski et al., 2011), electrochemical synthesis (Joaristi et al., 2012), mechanochemical synthesis (Klimakow et al., 2010) and sono-chemical synthesis (Son et al., 2008).

The most commonly used method to prepare MOF-based nanophotocatalyst is solvothermal synthesis. In solvothermal synthesis, MOF crystallizes out on mixing metal salt and ligand solutions or on adding a solvent to a mixture of solid salt and ligand.

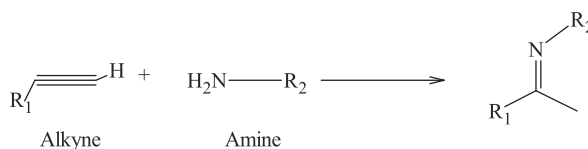
### Selective oxidation reactions



### Selective reduction reactions



### Addition reaction



**Scheme 6** Selective organic reactions photo-catalyzed by surface plasmon-mediated catalysts.

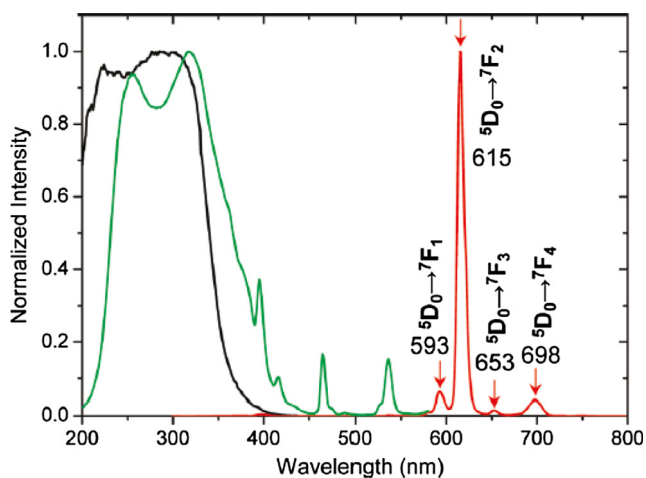


**Figure 12** Spectra of nanosized Eu-MOF powders in ambient atmosphere (Choi et al., 2010).

#### 4.1. Mechanism of photocatalytic activity for organic synthesis by MOF

MOFs are potentially good photocatalysts for organic transformations. These can be easily reused and recycled due to the heterogeneous characteristics. They also possess large surface area due to the microporous structure. The porous structure allows the easy movement of reactants and products in and out of the framework of the catalyst. Also the nanometer-sized pores facilitate the stabilization of intermediates by solvents because of confinement effect, thereby driving the reaction in the forward direction. The morphology and optical properties can be adjusted by varying the metal ions, metal clusters, bridging ligands and the anions in the metal salt precursor. For example,  $\text{Zn}_4\text{O}(\text{BDC})_6$  MOF (MOF-5) absorbs in 400 nm region of spectrum. The crystalline structure affords an easy study of the structure-property relationship, thus helping in modification of the catalyst (J.-L. Wang et al., 2012).

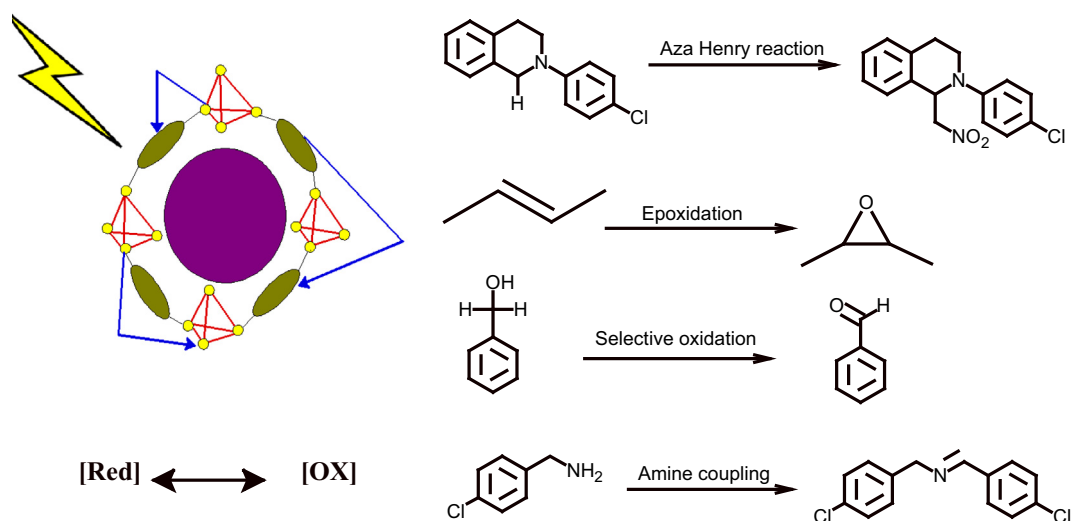
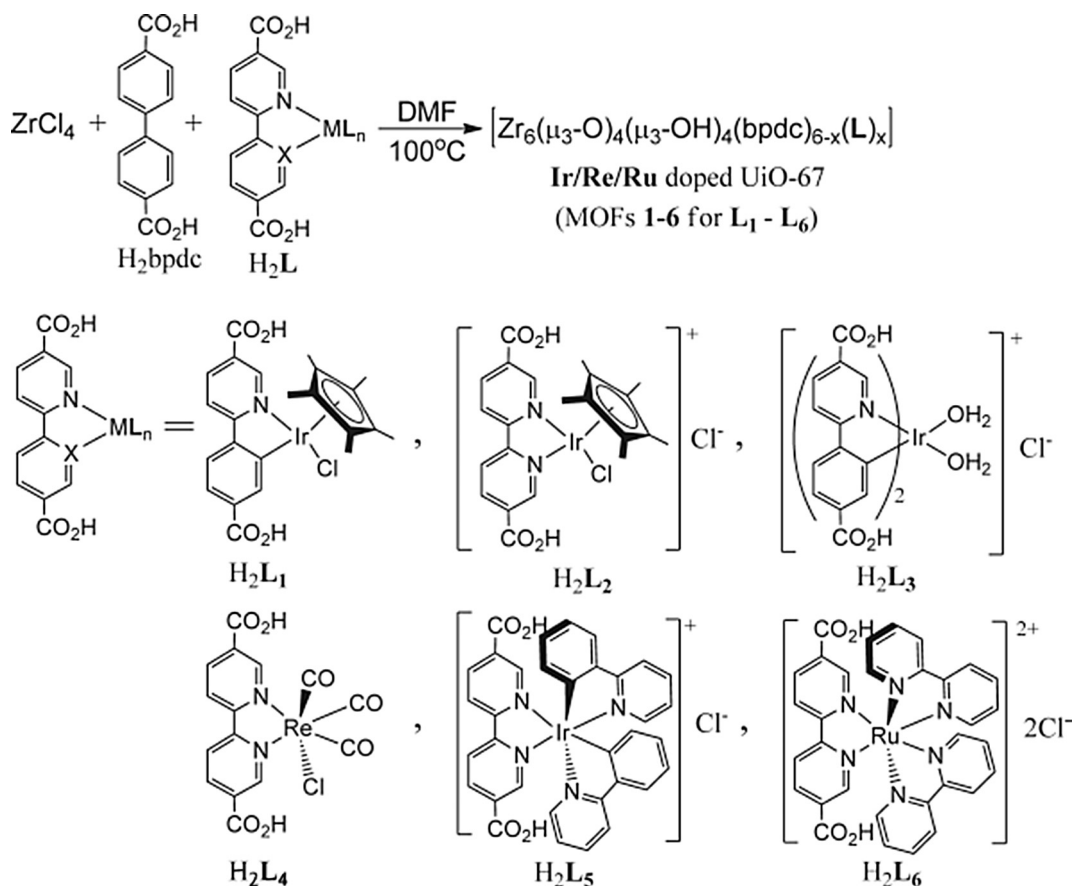


**Figure 13** Illustration of mechanism of action of MOF. Yellow spheres indicate the metal ions in the framework. Purple sphere indicates the substrate trapped in pore of MOF. Green ovals denote the bridging ligands. Blue arrows denote metal-metal, metal-ligand, ligand-ligand charge transfer on irradiation. [Ox] and [Red] denote oxidized and reduced species respectively.



**Scheme 7** Synthesis of doped UiO-67 (C. Wang et al., 2011).

For instance, the Eu-MOF with  $\text{Eu}^{3+}$  as the metal ion and 1,3,5-benzenetribenzoate (BTB) as the bridging ligand were reported to have a large BET surface area  $1001 \text{ m}^2/\text{g}$ . It possesses a porous structure with pore volume  $0.5 \text{ cm}^3/\text{g}$  and pore diameter of  $2 \text{ nm}$  (Choi et al., 2010). Spectral analysis of the

nanoparticles of the MOF indicated that when the ligand BTB was excited at  $285 \text{ nm}$ , emission lines at  $593$ ,  $615$ ,  $653$ , and  $698 \text{ nm}$ , corresponding to transitions in  $\text{Eu}^{3+}$ , were obtained (Fig. 12). This demonstrates an efficient ligand to metal energy transfer.

Hence, the mechanism of action of MOF involves absorption of radiation followed by metal-ligand, ligand-ligand or metal-metal energy or charge transfer (Fig. 13). The photogenerated  $e^-h^+$  pairs so formed can catalyze various redox organic transformations of molecules adsorbed on the MOF.

Yet, the main threat to the wide-spread applicability of the MOF is its low stability. The utility of MOF is limited by its tendency to undergo hydrolysis that can result in the collapse of its pore structure. This subsequently reduces the MOF photoactivity even under slight exposure to water despite the conditions being ambient (Greathouse and Allendorf, 2006). Hence the primary challenge in this field is to develop MOFs that are stable enough to give appreciable conversions photochemically.

#### 4.2. Selective organic transformations photocatalyzed by MOF

Stable MOF-based heterogeneous catalysts for catalyzing oxidation of water, reduction of  $CO_2$  and various organic reactions were reported for the first time by C. Wang et al. (2011). Such stable MOFs contain bulky ligands having extended conjugation. Doping with suitable ligands can be done for accomplishing modifications of the MOF properties. For instance, various Ir, Re and Ru complexes could easily be doped into the framework of UiO-67 ( $Zr_6O_4(OH)_4(bpdc)_6$ ) (bpdc: para-biphenyl-dicarboxylic acid) because of comparable ligand lengths of bpdc and doping ligands (Scheme 7).

The iridium complex doped UiO-67 and the ruthenium complex doped UiO-67 catalyzed the aza-Henry reaction between tertiary amines and nitroalkanes, on irradiation using 26 W fluorescent lamp for 12 h. The conversion rate was 59% and 86% respectively, with 1 mol% catalyst loading. The Ru complex based UiO-67 also catalyzed the aerobic oxidative coupling of amines and aerobic oxidation of thioanisole to methyl phenyl sulfoxide (sulfide to sulfoxide). The over-oxidized product sulfone was not detected in  $^1H$  NMR, implying that the catalyst is highly selective. The conversion of sulfide to sulfoxide did not take place in an atmosphere of  $N_2$ , indicating  $O_2$  to be the oxidizing agent. Also, on using methanol as a solvent, no electron relay or shuttle system was required. When the same reaction was carried out by using  $Ru(bpy)_3^{2+}$  as photocatalyst and acetonitrile as solvent, lead ruthenate pyrochlore mineral was required as a shuttle for electrons (Zen et al., 2003).

Another MOF based photocatalyst used in the oxidation of sulfides to sulfoxides using  $O_2$  as oxidant was Sn-MOF, with photoactive tin porphyrin ( $Sn^{IV}TPyP$ ) bridging ligand connecting the Zn atoms, which was further anchored by formate groups (Xie et al., 2011). The catalyst was also efficient for the conversion of 1,5-dihydroxynaphthalene to 5-hydroxynaphthalene-1,4-dione.

Zr based MOFs, Zr-benzenedicarboxylate (UiO-66) and its derivative, Zr-2- $NH_2$ -benzene-dicarboxylate (UiO-66( $NH_2$ )) were studied for their applicability in organic conversions. Long et al. (2012) developed UiO-66- $NH_2$  and studied it for the selective aerobic oxidations of compounds such as alcohols, olefins and cyclic alkanes. The MOF structure of the catalyst consisted of hexameric  $Zr_6O_32$  units and 2-aminoterephthalate as organic bridging linkers. The catalyst absorbed in the visible part of the spectrum ( $\lambda \geq 420$  nm), leading to HOMO-LUMO transition of electrons, which

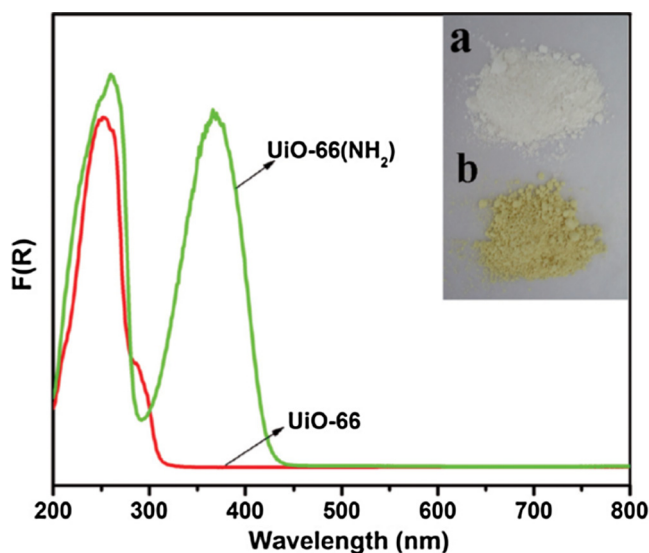
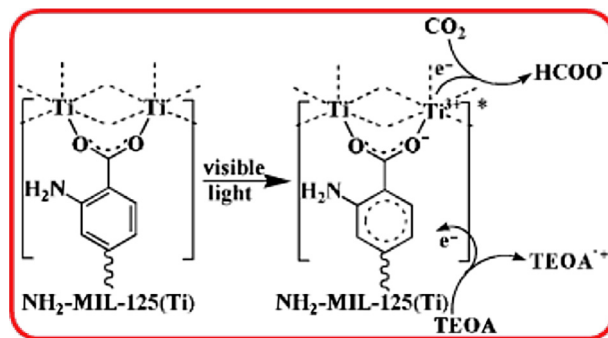


**Figure 14** UV-vis spectra of UiO-66 and UiO-66( $NH_2$ ); inset are the photographs of (a) UiO-66 (a) and (b) UiO-66( $NH_2$ ) (Shen et al., 2013).

generated  $e^-h^+$  pairs. These electrons reduced oxygen molecules adsorbed on  $Zr^{3+}$  to superoxide radicals ( $O_2^-$ ). Concomitantly, the holes oxidized the reactant adsorbed on the amine sites of MOF to carbocations. The final products were formed by the reaction of carbocations with superoxide radicals.

UiO-66- $NH_2$  was applied for various selective oxidation reactions of alkenes and yields obtained after 12 h of irradiation using visible light irradiation were compared. The activity and selectivity toward corresponding aldehyde/ketone or epoxide obtained were found to depend on the substrate and the solvent. Remarkably, the catalyst was of low activity for the selective oxidation of cyclooctene (conversion rate 0.8% to 0.5%, under different solvents). This was proposed to be due to the large kinetic diameter of the substrate relative to the pore size of catalyst. In view of the kinetic factors imposed by the porous structure of MOFs, we suggest that MOF based nanophotocatalysts can be developed for shape/size-selective photocatalysis in future.

Polar solvent like acetonitrile stabilized the intermediate epoxide more and resulted in higher conversion rates as



**Scheme 8** Mechanism of photocatalytic action of  $NH_2$ -Ti-based MOF (Fu et al., 2012).

compared to less polar solvents such as benzotrifluoride, N,N-dimethylformamide, chloroform and acetone. The catalyst was also studied for selective oxidation of alcohols to corresponding carbonyls. The oxidation took place with 100% selectivity toward carbonyl compounds. The ability of the catalyst to catalyze oxidation reaction decreased in the order benzyl alcohol > cyclohexanol > hexyl alcohol, parallel to an increase in the activation energy of  $\alpha$ -C-H bond. Also, under identical experimental conditions, these reactions did not take place in the presence of UiO-66 as catalyst, which further proved the importance of amine groups incorporated in the framework structure.

In another study, the effect of functionalization by introducing  $-\text{NH}_2$  group into the framework was further investigated (Shen et al., 2013). UiO-66 and UiO-66- $\text{NH}_2$  were prepared by solvothermal process and were applied to photocatalytic reactions. The activity of the catalyst UiO-66- $\text{NH}_2$  was compared with that of UiO-66. The catalyst UiO-66- $\text{NH}_2$  was effective in the oxidation of benzyl alcohol, substituted benzyl alcohol and other alcohols such as 3-methyl-2-buten-1-ol using benzene trifluoride solvent under visible-light irradiation. For example, using this catalyst, a conversion rate of 21% and selectivity greater than 99% could be attained for the conversion of benzyl alcohol to benzaldehyde. UiO-66, as it is, was quite ineffective for these conversions, under visible light irradiation. Thus the presence of  $-\text{NH}_2$  group augmented the absorption in the visible region of the framework as indicated by the UV-visible spectra without reducing the stability or recyclability of the catalyst (Fig. 14).

Another MOF based photocatalyst in which  $-\text{NH}_2$  group enhanced the visible light absorption is a Ti based MOF. In this MOF, 2-amino-benzene-1,4-dicarboxylate (bdc- $\text{NH}_2$ ) was introduced as the organic bridging ligand (Fu et al., 2012). It was reported to be the first instance in which a MOF could successfully reduce  $\text{CO}_2$  into formate anion  $\text{HCOO}^-$  (Scheme 8). The structural modifications could extent the wavelength of absorption of radiation to 550 nm. The mechanism involves charge transfer from ligand to metal followed by reduction of  $\text{CO}_2$ . Triethanolamine was used as the sacrificial agent. After 10 h of irradiation, Turn Over Number (TON) per Ti center was approximately 0.03. The obtained yield is low and the process involves triethanolamine, which is not economical and environmental friendly. Still, it opens up a new range of possibilities of reactions catalyzed by MOFs.

Zirconium-based metal-organic frameworks containing two different organic linkers, 2-amino-1,4-benzenedicarboxylate ( $\text{NH}_2$ -BDC) and 2-X-1,4-benzenedicarboxylate (X-BDC, X = H, F, Cl, Br), were used as visible light photocatalysts for selective oxidation of benzyl alcohol to benzaldehyde (Goh et al., 2015). The reaction was performed at 80 °C in the presence 26 W helical bulb as the visible light source. Zr-MOF consisting of  $\text{NH}_2$ -BDC and F-BDC linkers gave five times more conversion as compared to Zr-MOF with  $\text{NH}_2$ -BDC and H-BDC linkers. The substituent in the linker thus had a major impact on the conversion rate, because of its role in charge-transfer processes which in turn control the catalytic process.

In a breakthrough study, nanocomposite of iron-based metal-organic framework (MIL-53(Fe)) and graphene was prepared by one-pot solvothermal method. The nanocomposite

was applied for the selective oxidation of alcohols to aldehydes and ketones (Yang et al., 2016). The catalyst gave carbonyl compounds with high selectivity (99%). But the main distinctive feature of the catalyst was its high stability and reusability up to four cycles without any loss of catalytic activity.

Chirality can be introduced into MOF by incorporating an asymmetric organic entity in the framework. The MOFs so formulated can prove to be highly efficient stereoselective photocatalysts. For example L or D-stereoisomers of the organocatalyst pyrrolidin-2-yl-imidazole (PY1) were introduced along with photoactive triphenylamine into a MOF. This simultaneously equipped the two resulting MOFs (Zn-PY11 and Zn-PY12) with chirality and photoactivity. The chiral photocatalyst was studied for asymmetric  $\alpha$ -alkylation of aldehydes. On irradiation with a fluorescent lamp (26 W), in the presence of diethyl 2-bromomalonate as alkylating agent enantioselectivity of up to 92% was obtained after 24 h (Wu et al., 2012).

## 5. Conclusions and perspectives

In conclusion, this review discussed the preparation, mechanism and application of nanophotocatalysts in carrying out selective organic transformations. Furthermore, the plethora of nanophotocatalysts developed so far for organic conversions was classified based on their composition and mechanism, to make their study easier.

Though the literature survey revealed that progressive developments are being made to fabricate materials with improved photocatalytic properties, still a lot more research is desired in this field. Most importantly, the stability and the performance of these catalysts need to be monitored in natural sunlight. The catalysts have been prominently applied for selective oxidation of alcohols and reduction in nitroaromatics. There is no denying that these conversions were accompanied with high selectivities. Still, the scope of reactions for which these photocatalysts are being applied needs to be further widened. The catalytic activity was observed to depend mainly on the composition, nature of used support, size of nanoparticles, shape of nanoparticles, polarity of reactant, intensity of irradiation and the used solvent. These parameters need to be monitored and can be controlled to develop better photocatalysts.

Even though the literature is more abundant with the studies on graphene and semiconductor based nanocomposites, MOFs and plasmon-based photocatalysts are also fast emerging as potential nanophotocatalysts. Newer kinds of arrangements of components in the composites are being developed. The composites are being extended from binary to ternary structures. Further improvisations can be done by preparing composite materials of different classes of photocatalysts discussed in this review, where the distinct merits of each component can be tapped to the fullest.

It is beyond doubt that the conservation of earth's non-renewable resources is the need of the hour. The development of low-cost, stable nanophotocatalysts will open up new possibilities to convert solar energy to chemical energy and can prove to be an extremely important step toward solving the energy crisis of the world.

## References

- Alejo, C.J.B., D'Alfonso, C., Pacioni, N.L., Bejar, M.G., Grenier, M., Lanzalunga, O., Alarcon, E.I., Scaiano, J.C., 2012. Ultraclean derivatized monodisperse gold nanoparticles through laser drop ablation customization of polymorph gold nanostructures. *Langmuir* 28, 8183–8189.
- Ali, R., Nour, K., Al-warthan, A., Siddiqui, M.R.H., 2015. Selective oxidation of benzylic alcohols using copper-manganese mixed oxide nanoparticles as catalyst. *Arab. J. Chem.* 8, 512–517.

- An, C., Wang, J., Jiang, W., Zhang, M., Ming, X., Wang, S., Zhang, Q., 2012. Strongly visible-light responsive plasmonic shaped AgX: Ag (X = Cl, Br) nanoparticles for reduction of CO<sub>2</sub> to methanol. *Nanoscale* 4, 5646–5650.
- An, X., Yu, J.C., 2011. Graphene-based photocatalytic composites. *RSC Adv.* 1, 1426–1434.
- Avasthi, D.K., Mishra, Y.K., Singhal, R., Kabiraj, D., Mohapatra, S., Mohanta, B., Gohil, N.K., Singh, N., 2010. Synthesis of plasmonic nanocomposites for diverse applications. *J. Nanosci. Nanotechnol.* 10, 2705–2712.
- Bai, H., Li, C., Shi, G., 2011. Functional composite materials based on chemically converted graphene. *Adv. Mater.* 23, 1089–1115.
- Bandara, J., Mielczarski, J.A., Kiwi, J., 1999. Photosensitized degradation of azo dyes on Fe, Ti, and Al oxides. Mechanism of charge transfer during the degradation. *Langmuir* 15, 7680–7687.
- Bi, H., Zhao, W., Sun, S., Cui, H., Lin, T., Huang, F., Xie, X., Jiang, M., 2013. Graphene films decorated with metal sulfide nanoparticles for use as counter electrodes of dye-sensitized solar cells. *Carbon* 61, 116–123.
- Bickley, R.I., Munuera, G., Stone, F.S., 1973. Photoadsorption and photocatalysis at rutile surfaces: II. Photocatalytic oxidation of isopropanol. *J. Catal.* 31, 398–407.
- Chen, C., 2013. Visible Light Photocatalysts for Synthesis of Fine Organic Chemicals on Supported Nanostructures (Dissertation). Queensland University of Technology, Brisbane.
- Chen, C., Cai, W., Long, M., Zhou, B., Wu, Y., Wu, D., Feng, Y., 2010. Synthesis of visible-light responsive graphene oxide/TiO<sub>2</sub> composites with p/n heterojunction. *ACS Nano* 4, 6425–6432.
- Chen, C., Long, M., Xia, M., Zhang, C., Cai, W., 2012. Reduction of graphene oxide by an in-situ photoelectrochemical method in a dye-sensitized solar cell assembly. *Nanoscale Res. Lett.* 7, 101–105.
- Chen, F.-J., Cao, Y.-L., Jia, D.-Z., 2013. A room-temperature solid-state route for the synthesis of graphene oxide–metal sulfide composites with excellent photocatalytic activity. *CrystEngComm* 15, 4747–4754.
- Chen, Z., Liu, S., Yang, M.-Q., Xu, Y.-J., 2013. Synthesis of uniform CdS nanospheres/graphene hybrid nanocomposites and their application as visible light photocatalyst for selective reduction of nitro organics in water. *ACS Appl. Mater. Interfaces* 5, 4309–4319.
- Chen, Z., Xu, Y.-J., 2013. Ultrathin TiO<sub>2</sub> layer coated-CdS spheres core-shell nanocomposite with enhanced visible-light photoactivity. *ACS Appl. Mater. Interfaces* 5, 13353–13363.
- Choi, J.R., Tachikawa, T., Fujitsuka, M., Majima, T., 2010. Europium-based metal-organic framework as a photocatalyst for the one-electron oxidation of organic compounds. *Langmuir* 26, 10437–10443.
- Christopher, P., Ingram, D.B., Linic, S., 2010. Enhancing photochemical activity of semiconductor nanoparticles with optically active Ag nanostructures: photochemistry mediated by Ag surface plasmons. *J. Phys. Chem. C* 114, 9173–9177.
- Christopher, P., Linic, S., 2008. Engineering selectivity in heterogeneous catalysis: Ag nanowires as selective ethylene epoxidation catalysts. *J. Am. Chem. Soc.* 130, 11264–11265.
- Christopher, P., Linic, S., 2010. Shape- and size-specific chemistry of Ag nanostructures in catalytic ethylene epoxidation. *Chem-CatChem* 2, 78–83.
- Christopher, P., Xin, H., Linic, S., 2011. Visible-light-enhanced catalytic oxidation reactions on plasmonic silver nanostructures. *Nat. Chem.* 3, 467–472.
- Colmenares, J.C., Ouyang, W., Ojeda, M., Kuna, E., Chernyayeva, O., Lisovtyskiy, D., De, S., Luque, R., Balu, A.M., 2016. Mild ultrasound-assisted synthesis of TiO<sub>2</sub> supported on magnetic nanocomposites for selective photo-oxidation of benzyl alcohol. *Appl. Catal. B – Environ.* 183, 107–112.
- Curri, M.L., Comparelli, R., Cozzoli, P.D., Mascolo, G., Agostiano, A., 2003. Colloidal oxide nanoparticles for the photocatalytic degradation of organic dye. *Mater. Sci. Eng., C* 23, 285–289.
- Das, D.P., Barik, R.K., Das, J., Mohapatra, P., Parida, K.M., 2012. Visible light induced photo-hydroxylation of phenol to catechol over RGO–Ag<sub>3</sub>VO<sub>4</sub> nanocomposites without the use of H<sub>2</sub>O<sub>2</sub>. *RSC Adv.* 2, 7377–7379.
- Das, S., Sudhagar, P., Nagarajan, S., Ito, E., Lee, S.Y., Kang, Y.S., Choi, W., 2012. Synthesis of graphene-CoS electro-catalytic electrodes for dye sensitized solar cells. *Carbon* 50, 4815–4821.
- Ding, Y.H., Zhang, P., Ren, H.M., Zhuo, Q., Yang, Z.M., Jiang, Y., 2011. Preparation of graphene/TiO<sub>2</sub> anode materials for lithium-ion batteries by a novel precipitation method. *Mater. Res. Bull.* 46, 2403–2407.
- Du, A., Ng, Y.H., Bell, N.J., Zhu, Z., Amal, R., Smith, S.C., 2011. Hybrid graphene/titania nanocomposite: interface charge transfer, hole doping, and sensitization for visible light response. *J. Phys. Chem. Lett.* 2, 894–899.
- Du, D., Liu, J., Zhang, X., Cui, X., Lin, Y., 2011. One-step electrochemical deposition of a graphene-ZrO<sub>2</sub> nanocomposite: preparation, characterization and application for detection of organophosphorus agents. *J. Mater. Chem.* 21, 8032–8037.
- Du, J., Lai, X., Yang, N., Zhai, J., Kisailus, D., Su, F., Wang, D., Jiang, L., 2011. Hierarchically ordered macro-mesoporous TiO<sub>2</sub>–graphene composite films: improved mass transfer, reduced charge recombination, and their enhanced photocatalytic activities. *ACS Nano* 5, 590–596.
- Du, M., Li, C.-P., Zhao, X.-J., 2006. Metal-controlled assembly of coordination polymers with the flexible building block 4-pyridylacetic acid (Hpya). *Cryst. Growth Des.* 6, 335–341.
- Enache, D.I., Edwards, J.K., Landon, P., Solsona-Espriu, B., Carley, A.F., Herzing, A.A., Watanabe, M., Kiely, C.J., Knight, D.W., Hutchings, G.J., 2006. Solvent-free oxidation of primary alcohols to aldehydes using Au-Pd/TiO<sub>2</sub> catalysts. *Science* 311, 362–365.
- Eskandari, P., Kazemi, F., Zand, Z., 2014. Photocatalytic reduction of aromatic nitro compounds using CdS nanostructure under blue LED irradiation. *J. Photochem. Photobiol. A* 274, 7–12.
- Fan, J., Liu, E.-Z., Tian, L., Hu, X.-Y., He, Q., Sun, T., 2011. Synergistic effect of N and Ni<sup>2+</sup> on nanotitania in photocatalytic reduction of CO<sub>2</sub>. *J. Environ. Eng.* 137, 171–176.
- Feng, X., Sloppy, J.D., LaTempa, T.J., Paulose, M., Komarneni, S., Bao, N., Grimes, C.A., 2011. Synthesis and deposition of ultrafine Pt nanoparticles within high aspect ratio TiO<sub>2</sub> nanotube arrays: application to the photocatalytic reduction of carbon dioxide. *J. Mater. Chem.* 21, 13429–13433.
- Fu, Y., Sun, D., Chen, Y., Huang, R., Ding, Z., Fu, X., Li, Z., 2012. An amine-functionalized titanium metal-organic framework photocatalyst with visible-light-induced activity for CO<sub>2</sub> reduction. *Angew. Chem. Int. Ed.* 51, 3364–3367.
- Fujishima, A., Honda, K., 1972. Electrochemical photolysis of water at a semiconductor electrode. *Nature* 238, 37–38.
- Fujishima, A., Rao, T.N., Tryk, D.A., 2000. Titanium dioxide photocatalysis. *J. Photochem. Photobiol. C: Photochem. Rev.* 1, 1–21.
- Gao, E., Wang, W., Shang, M., Xu, J., 2011. Synthesis and enhanced photocatalytic performance of graphene-Bi<sub>2</sub>WO<sub>6</sub> composite. *Phys. Chem. Chem. Phys.* 13, 2887–2893.
- Geng, X., Niu, L., Xing, Z., Song, R., Liu, G., Sun, M., Cheng, G., Zhong, H., Liu, Z., Zhang, Z., Sun, L., Xu, H., Lu, L., Liu, L., 2010. Aqueous-processable noncovalent chemically converted graphene–quantum dot composites for flexible and transparent optoelectronic films. *Adv. Mater.* 22, 638–642.
- Goh, T.W., Xiao, C., Maligal-Ganesh, R.V., Li, X., Huang, W., 2015. Utilizing mixed-linker zirconium based metal-organic frameworks to enhance the visible light photocatalytic oxidation of alcohol. *Chem. Eng. J.* 124, 45–51.
- Greathouse, J.A., Allendorf, M.D., 2006. The interaction of water with MOF-5 simulated by molecular dynamics. *J. Am. Chem. Soc.* 128, 10678–10679.
- Grirrane, A., Corma, A., Garcia, H., 2009. Highly active and selective gold catalysts for the aerobic oxidative condensation of benzy-

- lamines to imines and one-pot, two-step synthesis of secondary benzylamines. *J. Catal.* 264, 138–144.
- Guo, H., Kemell, M., Al-Hunaiti, A., Rautiainen, S., Leskela, M., Repo, T., 2011. Gold-palladium supported on porous steel fiber matrix: structured catalyst for benzyl alcohol oxidation and benzyl amine oxidation. *Catal. Commun.* 12, 1260–1264.
- Guo, J., Zhu, S., Chen, Z., Li, Y., Yu, Z., Liu, Q., Li, J., Feng, C., Zhang, D., 2011. Sonochemical synthesis of TiO<sub>2</sub> nanoparticles on graphene for use as photocatalyst. *Ultrason. Sonochem.* 18, 1082–1090.
- Harada, H., Sakata, T., Ueda, T., 1989. Semiconductor effect on the selective photocatalytic reaction of .alpha.-hydroxycarboxylic acids. *J. Phys. Chem.* 93, 1542–1548.
- He, D., Li, Y., Wang, J., Yang, Y., An, Q., 2016. Tunable nanostructure of TiO<sub>2</sub>/reduced graphene oxide composite for high photocatalysis. *Appl. Microsc.* 46, 37–44.
- Hoffman, A.J., Mills, G., Yee, H., Hoffmann, M.R., 1992. Q-sized cadmium sulfide: synthesis, characterization, and efficiency of photoinitiation of polymerization of several vinylic monomers. *J. Phys. Chem.* 96, 5546–5552.
- Hsiao, M.-C., Liao, S.-H., Yen, M.-Y., Liu, P.-I., Pu, N.-W., Wang, C.-A., Ma, C.-C.M., 2010. Preparation of covalently functionalized graphene using residual oxygen-containing functional groups. *ACS Appl. Mater. Interfaces* 2, 3092–3099.
- Hsu, H.-C., Shown, I., Wei, H.-Y., Chang, Y.-C., Du, H.-Y., Lin, Y.-G., Tseng, C.-A., Wang, C.-H., Chen, L.-C., Lin, Y.-C., Chen, K. H., 2013. Graphene oxide as a promising photocatalyst for CO<sub>2</sub> to methanol conversion. *Nanoscale* 5, 262–268.
- Huang, X.Q., Li, Y.J., Chen, Y., Zhou, H.L., Duan, X.F., Huang, Y., 2013. Plasmonic and catalytic AuPd nanowheels for the efficient conversion of light into chemical energy. *Angew. Chem. Int. Ed.* 52, 6063–6067.
- Huang, Y., Qin, Y., Zhou, Y., Niu, H., Yu, Z.-Z., Dong, J.-Y., 2010. Polypropylene/graphene oxide nanocomposites prepared by in situ Ziegler–Natta polymerization. *Chem. Mater.* 22, 4096–4102.
- Hubsch, B., Mahieu, B., 1985. Conversion of dextrose into hydrogen using aqueous tris(2,2′-bipyridine)rhodium(III) complex as a photocatalyst and enhanced by efficient heterogeneous redox catalysts. *Polyhedron* 4, 669–674.
- Inoue, Y., 2009. Photocatalytic water splitting by RuO<sub>2</sub>-loaded metal oxides and nitrides with d<sup>0</sup>- and d<sup>10</sup>-related electronic configurations. *Energy Environ. Sci.* 2, 364–386.
- Jeong, H.-C., Shim, I.I.-W., Choi, K.Y., Lee, J.K., Park, J.-N., Lee, C.W., 2005. Hydroxylation of phenol with H<sub>2</sub>O<sub>2</sub> over transition metal containing nano-sized hollow core mesoporous shell carbon catalyst. *Korean J. Chem. Eng.* 22, 657–660.
- Jiang, H., Liu, Y., Zang, S., Li, J., Wang, H., 2015. Microwave-assisted hydrothermal synthesis of Nd, N, and P tri-doped TiO<sub>2</sub> from TiCl<sub>4</sub> hydrolysis and synergetic mechanism for enhanced photoactivity under simulated sunlight irradiation. *Mater. Sci. Semicond. Proc.* 40, 822–831.
- Jiang, Z., Wang, C., Du, G., Zhong, Y.J., Jiang, J.Z., 2012. In situ synthesis of SnS<sub>2</sub> @ graphene nanocomposites for rechargeable lithium batteries. *J. Mater. Chem.* 22, 9494–9496.
- Jianwei, C., Jianwen, S., Xu, W., Haojie, C., Minglai, F., 2013. Recent progress in the preparation and application of semiconductor/graphene composite photocatalysts. *Chin. J. Catal.* 34, 621–640.
- Joaristi, A.M., Juan-Alcaniz, J., Serra-Crespo, P., Kapteijn, F., Gascon, J., 2012. Electrochemical synthesis of some archetypical Zn<sup>2+</sup>, Cu<sup>2+</sup>, and Al<sup>3+</sup> metal organic frameworks. *Cryst. Growth Des.* 12, 3489–3498.
- Kamat, P.V., 2010. Graphene based nanoarchitectures. Anchoring semiconductor and metal nanoparticles on a 2-dimensional carbon support. *J. Phys. Chem. Lett.* 1, 520–527.
- Kamat, P.V., Gevaert, M., Vinodgopal, K., 1997. Photochemistry on semiconductor surfaces. Visible light induced oxidation of C<sub>60</sub> on TiO<sub>2</sub> nanoparticles. *J. Phys. Chem. B* 101, 4422–4427.
- Kamat, P.V., Patrick, B., 1992. Photophysics and photochemistry of quantized ZnO colloids. *J. Phys. Chem.* 96, 6829–6834.
- Kaur, P., Bansal, P., Sud, D., 2013. Heterostructured nanophotocatalysts for degradation of organophosphate pesticides from aqueous streams. *J. Korean Chem. Soc.* 57, 382–388.
- Kawai, T., Sakata, T., 1980. Photocatalytic decomposition of gaseous water over TiO<sub>2</sub> and TiO<sub>2</sub>–RuO<sub>2</sub> surfaces. *Chem. Phys. Lett.* 72, 87–89.
- Ke, X., Sarina, S., Zhao, J., Zhang, X., Chang, J., Zhu, H., 2012. Tuning the reduction power of supported gold nanoparticle photocatalysts for selective reductions by manipulating wavelength of visible light irradiation. *Chem. Commun.* 48, 3509–3511.
- Ke, X., Zhang, X., Zhao, J., Sarina, S., Barry, J., Zhu, H., 2013. Selective reductions using visible light photocatalysts of supported gold nanoparticles. *Green Chem.* 15, 236–244.
- Kim, Y.-T., Han, J.-H., Hong, B.H., Kwon, Y.-U., 2010. Electrochemical synthesis of CdSe quantum-dot arrays on a graphene basal plane using mesoporous silica thin-film templates. *Adv. Mater.* 22, 515–518.
- Klimakow, M., Klobes, P., Thunemann, A.F., Rademann, K., Emmerling, F., 2010. Mechanochemical synthesis of metal–organic frameworks: a fast and facile approach toward quantitative yields and high specific surface areas. *Chem. Mater.* 22, 5216–5221.
- Klinowski, J., Paz, F.A.A., Silva, P., Rocha, J., 2011. Microwave-assisted synthesis of metal-organic frameworks. *Dalton Trans.* 40, 321–330.
- Kochuveedu, S.T., Kim, D.-P., Kim, D.H., 2012. Surface-plasmon-induced visible light photocatalytic activity of TiO<sub>2</sub> nanospheres decorated by Au nanoparticles with controlled configuration. *J. Phys. Chem. C* 116, 2500–2506.
- Kominami, H., Yamamoto, S., Imamura, K., Tanaka, A., Hashimoto, K., 2014. Photocatalytic chemoselective reduction of epoxides to alkenes along with formation of ketones in alcoholic suspensions of silver-loaded titanium(IV) oxide at room temperature without the use of reducing gases. *Chem. Commun.* 50, 4558–4560.
- Krishnamoorthy, K., Veerapandian, M., Yun, K., Kim, S.-J., 2013. The chemical and structural analysis of graphene oxide with different degrees of oxidation. *Carbon* 53, 38–49.
- Kulkarni, A.A., Bhanage, B.M., 2014. Ag@AgCl nanomaterial synthesis using sugar cane juice and its application in degradation of azo dyes. *ACS Sustain. Chem. Eng.* 2, 1007–1013.
- Kumar, P., Kumar, A., Sreedhar, B., Sain, B., Ray, S.S., Jain, S.L., 2014a. Cobalt Phthalocyanine immobilized on graphene oxide: an efficient visible-active catalyst for the photoreduction of carbon dioxide. *Chem. Eur. J.* 20, 6154–6161.
- Kumar, P., Sain, B., Jain, S.L., 2014b. Photocatalytic reduction of carbon dioxide to methanol using a ruthenium trinuclear polyazine complex immobilized on graphene oxide under visible light irradiation. *J. Mater. Chem. A* 2, 11246–11253.
- Kumar, P., Singh, P.K., Bhattacharya, B., 2011. Study of nano-CdS prepared in methanolic solution and polymer electrolyte matrix. *Ionics* 17, 721–725.
- Kumar, S.G., Devi, L.G., 2011. Review on modified TiO<sub>2</sub> photocatalysis under UV/visible light: selected results and related mechanisms on interfacial charge carrier transfer dynamics. *J. Phys. Chem. A* 115, 13211–13241.
- Kumbhar, P.S., Sanchez-Valente, J., Millet, J.M.C., Figueras, F., 2000. Mg–Fe hydroxalcite as a catalyst for the reduction of aromatic nitro compounds with hydrazine hydrate. *J. Catal.* 191, 467–473.
- Kuzmenko, A.B., van Heumen, E., Carbone, F., van der Marel, D., 2008. Universal optical conductance of graphite. *Phys. Rev. Lett.* 100, 117401–117404.
- Lambert, T.N., Chavez, C.A., Hernandez-Sanchez, B., Lu, P., Bell, N.S., Ambrosini, A., Friedman, T., Boyle, T.J., Wheeler, D.R., Huber, D.L., 2009. Synthesis and characterization of titania–graphene nanocomposites. *J. Phys. Chem. C* 113, 19812–19823.

- Larson, R.A., Stackhouse, P.L., Crowley, T.O., 1992. Riboflavin tetraacetate: a potentially useful photosensitizing agent for treatment of contaminated waters. *Environ. Sci. Technol.* 26, 1792–1798.
- Li, J., Cushing, S.K., Bright, J., Meng, F., Senty, T.R., Zheng, P., Bristow, A.D., Wu, N., 2013. Ag@Cu<sub>2</sub>O core-shell nanoparticles as visible-light plasmonic photocatalysts. *ACS Catal.* 3, 47–51.
- Li, J., Li, B., Li, J., Liu, J., Wang, L., Zhang, H., Zhang, Z., Zhao, B., 2015. Visible-light-driven photocatalyst of La–N-codoped TiO<sub>2</sub> nano-photocatalyst: fabrication and its enhanced photocatalytic performance and mechanism. *J. Ind. Eng. Chem.* 25, 16–21.
- Li, J., Yang, J., Wen, F., Li, C., 2011. A visible-light-driven transfer hydrogenation on CdS nanoparticles combined with iridium complexes. *Chem. Commun.* 47, 7080–7082.
- Li, N., Liu, G., Zhen, C., Li, F., Zhang, L., Cheng, H.-M., 2011. Battery performance and photocatalytic activity of mesoporous anatase TiO<sub>2</sub> nanospheres/graphene composites by template-free self-assembly. *Adv. Funct. Mater.* 21, 1717–1722.
- Li, Q., Guo, B., Yu, J., Ran, J., Zhang, B., Yan, H., Gong, J.R., 2011. Highly efficient visible-light-driven photocatalytic hydrogen production of CdS-cluster-decorated graphene nanosheets. *J. Am. Chem. Soc.* 133, 10878–10884.
- Liang, Y.T., Vijayan, B.K., Gray, K.A., Hersam, M.C., 2011. Minimizing graphene defects enhances titania nanocomposite-based photocatalytic reduction of CO<sub>2</sub> for improved solar fuel production. *Nano Lett.* 11, 2865–2870.
- Liao, G., Chen, S., Quan, X., Yu, H., Zhao, H., 2012. Graphene oxide modified g-C<sub>3</sub>N<sub>4</sub> hybrid with enhanced photocatalytic capability under visible light irradiation. *J. Mater. Chem.* 22, 2721–2726.
- Lightcap, I.V., Kosel, T.H., Kamat, P.V., 2010. Anchoring semiconductor and metal nanoparticles on a two-dimensional catalyst mat. Storing and shuttling electrons with reduced graphene oxide. *Nano Lett.* 10, 577–583.
- Lin, C., Tao, K., Hua, D., Ma, Z., Zhou, S., 2013. Size effect of gold nanoparticles in catalytic reduction of *p*-nitrophenol with NaBH<sub>4</sub>. *Molecules* 18, 12609–12620.
- Linic, S., Christopher, P., Xin, H., Marimuthu, A., 2013. Catalytic and photocatalytic transformations on metal nanoparticles with targeted geometric and plasmonic properties. *Acc. Chem. Res.* 46, 1890–1899.
- Liu, C., Lin, H., Gao, S., Yin, P., Guo, L., Huang, B., Dai, Y., 2014. AgI/AgCl/H<sub>2</sub>WO<sub>4</sub> double heterojunctions composites: preparation and visible-light photocatalytic performance. *Bull. Korean Chem. Soc.* 35, 441–447.
- Liu, E., Kang, L., Wu, F., Sun, T., Hu, X., Yang, Y., Liu, H., Fan, J., 2014. Photocatalytic reduction of CO<sub>2</sub> into methanol over Ag/TiO<sub>2</sub> nanocomposites enhanced by surface plasmon resonance. *Plasmonics* 9, 61–70.
- Liu, L., Ouyang, S., Ye, J., 2013. Gold-nanorod-photosensitized titanium dioxide with wide-range visible-light harvesting based on localized surface plasmon resonance. *Angew. Chem. Int. Ed.* 52, 6689–6693.
- Liu, C., Chen, Z., Zhang, N., Tang, Z.-R., Xu, Y.-J., 2013. An efficient self-assembly of CdS nanowires-reduced graphene oxide nanocomposites for selective reduction of nitro organics under visible light irradiation. *J. Phys. Chem. C* 117, 8251–8261.
- Liu, S., Yang, M.-Q., Zhang, N., Xu, Y.-J., 2014. Nanocomposites of graphene-CdS as photoactive and reusable catalysts for visible-light-induced selective reduction process. *J. Energy Chem.* 23, 145–155.
- Liu, S., Zhang, N., Tang, Z.-R., Xu, Y.-J., 2012. Synthesis of one-dimensional CdS @ TiO<sub>2</sub> core-shell nanocomposites photocatalyst for selective redox: the dual role of TiO<sub>2</sub> Shell. *ACS Appl. Mater. Interfaces* 4, 6378–6385.
- Liu, X., Pan, L., Lv, T., Zhu, G., Sun, Z., Sun, C., 2011. Microwave-assisted synthesis of CdS-reduced graphene oxide composites for photocatalytic reduction of Cr(VI). *Chem. Commun.* 47, 11984–11986.
- Long, J., Wang, S., Ding, Z., Wang, S., Zhou, Y., Huang, L., Wang, X., 2012. Amine-functionalized zirconium metal-organic framework as efficient visible-light photocatalyst for aerobic organic transformations. *Chem. Commun.* 48, 11656–11658.
- Long, M., Qin, Y., Chen, C., Guo, X., Tan, B., Cai, W., 2013. Origin of visible light photoactivity of reduced graphene oxide/TiO<sub>2</sub> by in situ hydrothermal growth of undergrown TiO<sub>2</sub> with graphene oxide. *J. Phys. Chem. C* 117, 16734–16741.
- Lv, X.-J., Fu, W.-F., Hu, C.-Y., Chen, Y., Zhou, W.-B., 2013. Photocatalytic reduction of CO<sub>2</sub> with H<sub>2</sub>O over a graphene-modified NiO<sub>x</sub>-Ta<sub>2</sub>O<sub>5</sub> composite photocatalyst: coupling yields of methanol and hydrogen. *RSC Adv.* 3, 1753–1757.
- Maeda, K., Domen, K., 2010. Photocatalytic water splitting: recent progress and future challenges. *J. Phys. Chem. Lett.* 1, 2655–2661.
- Maldotti, A., Molinari, A., Amadelli, R., 2002. Photocatalysis with organized systems for the oxofunctionalization of hydrocarbons by O<sub>2</sub>. *Chem. Rev.* 102, 3811–3836.
- Mangrulkar, P.A., Polshettiwar, V., Labhsetwar, N.K., Varma, R.S., Rayalu, S.S., 2012. Nano-ferrites for water splitting: unprecedented high photocatalytic hydrogen production under visible light. *Nanoscale* 4, 5202–5209.
- Matsumura, M., Furukawa, S., Saho, Y., Tsubomura, H., 1985. Cadmium sulfide photocatalyzed hydrogen production from aqueous solutions of sulfite: effect of crystal structure and preparation method of the catalyst. *J. Phys. Chem.* 89, 1327–1329.
- Matsumura, M., Hiramoto, M., Iehara, T., Tsubomura, H., 1984. Photocatalytic and photoelectrochemical reactions of aqueous solutions of formic acid, formaldehyde, and methanol on platinumized cadmium sulfide powder and at a cadmium sulfide electrode. *J. Phys. Chem.* 88, 248–250.
- McNaught, A.D., Wilkinson, A., 1997. IUPAC. Compendium of Chemical Terminology, second ed. Blackwell Scientific Publications, Oxford, UK.
- Meng, X., Geng, D., Liu, J., Li, R., Sun, X., 2011. Controllable synthesis of graphene-based titanium dioxide nanocomposites by atomic layer deposition. *Nanotechnology* 22, 165602.
- Mie, G., 1908. Beiträge zur Optik trüber Medien, speziell kolloidaler Metallösungen. *Ann. Phys.* 25, 377–445.
- Moores, A., Goettmann, F., 2006. The plasmon band in noble metal nanoparticles: an introduction to theory and applications. *New J. Chem.* 30, 1121–1132.
- Mori, K., Kawashima, M., Che, M., Yamashita, H., 2010. Enhancement of the photoinduced oxidation activity of a ruthenium(II) complex anchored on silica-coated silver nanoparticles by localized surface plasmon resonance. *Angew. Chem. Int. Ed.* 49, 8598–8601.
- Mukherji, A., Seger, B., Lu, G.Q., Wang, L., 2011. Nitrogen doped Sr<sub>2</sub>Ta<sub>2</sub>O<sub>7</sub> coupled with graphene sheets as photocatalysts for increased photocatalytic hydrogen production. *ACS Nano* 5, 3483–3492.
- Naik, B., Kim, S.M., Jung, C.H., Moon, S.Y., Kim, S.H., Park, J.Y., 2014. *Adv. Mater. Interfaces* 1, 1300018.
- Naya, S.-i., Inoue, A., Tada, H., 2010. Self-assembled hetero-supramolecular visible light photocatalyst consisting of gold nanoparticle-loaded titanium(IV) dioxide and surfactant. *J. Am. Chem. Soc.* 132, 6292–6293.
- Nedeljkovic, J.M., Nenadovic, M.T., Micic, O.I., Nozik, A.J., 1986. Enhanced photoredox chemistry in quantized semiconductor colloids. *J. Phys. Chem.* 90, 12–13.
- Neppolian, B., Bruno, A., Bianchi, C.L., Ashokkumar, M., 2012. Graphene oxide based Pt-TiO<sub>2</sub> photocatalyst: ultrasound assisted synthesis, characterization and catalytic efficiency. *Ultrason. Sonochem.* 19, 9–15.
- Neubauer, A., Grell, G., Friedrich, A., Bokarev, S.I., Schwarzbach, P., Gartner, F., Surkus, A.-E., Junge, H., Beller, M., Kuhn, O., Lochbrunner, S., 2014. Electron- and energy-transfer processes in a

- photocatalytic system based on an Ir(III)-photosensitizer and an iron catalyst. *J. Phys. Chem. Lett.* 5, 1355–1360.
- Ng, Y.H., Lightcap, I.V., Goodwin, K., Matsumura, M., Kamat, P. V., 2010. To what extent do graphene scaffolds improve the photovoltaic and photocatalytic response of TiO<sub>2</sub> nanostructured films? *J. Phys. Chem. Lett.* 1, 2222–2227.
- Novoselov, K.S., Geim, A.K., Morozov, S.V., Jiang, D., Zhang, Y., Dubonos, S.V., Grigorieva, I.V., Firsov, A.A., 2004. Electric field effect in atomically thin carbon films. *Science* 306, 666–669.
- Ohno, T., Higo, T., Murakami, N., Saito, H., Zhang, Q., Yang, Y., Tsubota, T., 2014. Photocatalytic reduction of CO<sub>2</sub> over exposed-crystal-face-controlled TiO<sub>2</sub> nanorod having a brookite phase with co-catalyst loading. *Appl. Catal. B – Environ.* 152–153, 309–316.
- Ola, O., Maroto-Valer, M., 2011. Role of catalyst carriers in CO<sub>2</sub> photoreduction over nanocrystalline nickel loaded TiO<sub>2</sub>-based photocatalysts. *J. Catal.* 309, 300–308.
- Pachfule, P., Das, R., Poddar, P., Banerjee, R., 2011. Solvothermal synthesis, structure, and properties of metal organic framework isomers derived from a partially fluorinated link. *Cryst. Growth Des.* 11, 1215–1222.
- Paek, S.M., Yoo, E., Honma, I., 2009. Enhanced cyclic performance and lithium storage capacity of SnO<sub>2</sub>/graphene nanoporous electrodes with three-dimensionally delaminated flexible structure. *Nano Lett.* 9, 72–75.
- Palmisano, G., Augugliaro, V., Pagliaro, M., Palmisano, L., 2007. Photocatalysis: a promising route for 21st century organic chemistry. *Chem. Commun.*, 3425–3437
- Park, J.Y., Kim, S.M., Lee, H., Naik, B., 2014. Hot electron and surface plasmon-driven catalytic reaction in metal–semiconductor nanostructures. *Catal. Lett.* 144, 1996–2004.
- Park, S., An, J., Jung, I., Piner, R.D., An, S.J., Li, X., Velamakanni, A., Ruoff, R.S., 2009. Colloidal suspensions of highly reduced graphene oxide in a wide variety of organic solvents. *Nano Lett.* 9, 1593–1597.
- Poole Jr., C.P., Owens, F.J., 2003. *Introduction to Nanotechnology*. John Wiley & Sons Inc., Hoboken, New Jersey.
- Qiu, B., Zhou, Y., Ma, Y., Yang, X., Sheng, W., Xing, M., Zhang, J., 2015. Facile synthesis of the Ti<sup>3+</sup> self-doped TiO<sub>2</sub>-graphene nanosheet composites with enhanced photocatalysis. *Sci. Rep.* 5, 8591.
- Ravelli, D., Dondi, D., Fagnoni, M., Albin, A., 2009. Photocatalysis. A multi-faceted concept for green chemistry. *Chem. Soc. Rev.* 38, 1999–2011.
- Ren, Z., Zhang, J., Xiao, F.-X., Xiao, G., 2014. Revisiting the construction of graphene–CdS nanocomposites as efficient visible-light-driven photocatalysts for selective organic transformation. *J. Mater. Chem. A* 2, 5330–5339.
- Roduner, E., 2006. Size matters: why nanomaterials are different. *Chem. Soc. Rev.* 35, 583–592.
- Roy, P., Periasamy, A.P., Liang, C.T., Chang, H.T., 2013. Synthesis of graphene-ZnO-Au nanocomposites for efficient photocatalytic reduction of nitrobenzene. *Environ. Sci. Technol.* 47, 6688–6695.
- Rozhkova, E.A., Ulasov, I., Lai, B., Dimitrijevic, N.M., Lesniak, M. S., Rajh, T., 2009. A high-performance nanobio photocatalyst for targeted brain cancer therapy. *Nano Lett.* 9, 3337–3342.
- Sathishkumar, P., Sweena, R., Wu, J.J., Anandan, S., 2011. Synthesis of CuO-ZnO nanophotocatalyst for visible light assisted degradation of a textile dye in aqueous solution. *Chem. Eng. J.* 171, 136–140.
- Selvam, K., Balachandran, S., Velmurugan, R., Swaminathan, M., 2012. Mesoporous nitrogen doped nano titania—a green photocatalyst for the effective reductive cleavage of azoxybenzenes to amines or 2-phenyl indazoles in methanol. *Appl. Catal. A* 413–414, 213–222.
- Selvam, K., Krishnakumar, B., Velmurugan, R., Swaminathan, M., 2009. A simple one pot nano titania mediated green synthesis of 2-alkylbenzimidazoles and indazole from aromatic azides under UV and solar light. *Catal. Commun.* 11, 280–284.
- Selvam, K., Swaminathan, M., 2010. Au-doped TiO<sub>2</sub> nanoparticles for selective photocatalytic synthesis of quinaldines from anilines in ethanol. *Tetrahedron Lett.* 51, 4911–4914.
- Selvam, K., Swaminathan, M., 2011. An easy one-step photocatalytic synthesis of 1-aryl-2-alkylbenzimidazoles by platinum loaded TiO<sub>2</sub> nanoparticles under UV and solar light. *Tetrahedron Lett.* 52, 3386–3392.
- Selvam, K., Swaminathan, M., 2012. Nano N-TiO<sub>2</sub> mediated selective photocatalytic synthesis of quinaldines from nitrobenzenes. *RSC Adv.* 2, 2848–2855.
- Sheldon, R.A., Arends, I.W.C.E., ten Brink, G.J., Dijkstra, A., 2002. Green, catalytic oxidations of alcohols. *Acc. Chem. Res.* 35, 774–781.
- Shen, J., Shi, M., Yan, B., Ma, H., Li, N., Ye, M., 2011. Ionic liquid-assisted one-step hydrothermal synthesis of TiO<sub>2</sub>-reduced graphene oxide composites. *Nano Res.* 4, 795–806.
- Shen, L., Liang, S., Wu, W., Liang, R., Wu, L., 2013. Multifunctional NH<sub>2</sub>-mediated zirconium metal-organic framework as an efficient visible-light-driven photocatalyst for selective oxidation of alcohols and reduction of aqueous Cr(VI). *Dalton Trans.* 42, 13649–13657.
- Shi, G., Mao, Y., Ren, G., Gong, L., Zhi, Z., 2014. Synthesis and photolysis of NaYF<sub>4</sub>@SiO<sub>2</sub>@TiO<sub>2</sub> core-shell nanocomposites. *Opt. Commun.* 332, 219–222.
- Shrivastava, K., 2009. *Study of Photocatalytic Organic Functional Transformations by Metal CdS Composite Particles (Dissertation)*. Thapar University, Patiala.
- Shu, W., Liu, Y., Peng, Z., Chen, K., Zhang, C., Chen, W., 2013. Synthesis and photovoltaic performance of reduced graphene oxide–TiO<sub>2</sub> nanoparticles composites by solvothermal method. *J. Alloys Compd.* 563, 229–233.
- Siddiq, A., Masih, D., Anjum, D., Siddiq, M., 2015. Cobalt and sulfur co-doped nano-size TiO<sub>2</sub> for photodegradation of various dyes and phenol. *J. Environ. Sci.* 37, 100–109.
- Somorjai, G.A., Frei, H., Park, J.Y., 2009. Advancing the frontiers in nanocatalysis, biointerfaces, and renewable energy conversion by innovations of surface techniques. *J. Am. Chem. Soc.* 131, 16589–16605.
- Son, W.-J., Kim, J., Kim, J., Ahn, W.-S., 2008. Sonochemical synthesis of MOF-5. *Chem. Commun.* 47, 6336–6338.
- Stengl, V., Popelkova, D., Vlácil, P., 2011. TiO<sub>2</sub>-graphene nanocomposite as high performance photocatalysts. *J. Phys. Chem. C* 115, 25209–25218.
- Stibal, D., Sa, J., van Bokhoven, J.A., 2013. One-pot photo-reductive N-alkylation of aniline and nitroarene derivatives with primary alcohols over Au–TiO<sub>2</sub>. *Catal. Sci. Technol.* 3, 94–98.
- Stoller, M.D., Park, S., Zhu, Y., An, J., Ruoff, R.S., 2008. Graphene-based ultracapacitors. *Nano Lett.* 8, 3498–3502.
- Su, Y., Wang, L.C., Liu, Y.M., Cao, Y., He, H.-Y., Fan, K.N., 2007. Microwave-accelerated solvent-free aerobic oxidation of benzyl alcohol over efficient and reusable manganese oxides. *Catal. Commun.* 8, 2181–2185.
- Sun, L., Shao, R., Tang, L., Chen, Z., 2013. Synthesis of ZnFe<sub>2</sub>O<sub>4</sub>/ZnO nanocomposites immobilized on graphene with enhanced photocatalytic activity under solar light irradiation. *J. Alloys Compd.* 564, 55–62.
- Sun, S., Gao, L., Liu, Y., 2010. Enhanced dye-sensitized solar cell using graphene-TiO<sub>2</sub> photoanode prepared by heterogeneous coagulation. *Appl. Phys. Lett.* 96, 083113.
- Sun, Z., James, D.K., Tour, J.M., 2011. Graphene chemistry: synthesis and manipulation. *J. Phys. Chem. Lett.* 2, 2425–2432.
- Tanaka, A., Hashimoto, K., Kominami, H., 2011. Selective photocatalytic oxidation of aromatic alcohols to aldehydes in an aqueous suspension of gold nanoparticles supported on cerium(IV) oxide under irradiation of green light. *Chem. Commun.* 47, 10446–10448.
- Tanaka, A., Ogino, A., Iwaki, M., Hashimoto, K., Ohnuma, A., Amano, F., Ohtani, B., Kominami, H., 2012. Gold-titanium(IV) oxide plasmonic photocatalysts prepared by a colloid-photodepo-

- sition method: correlation between physical properties and photocatalytic activities. *Langmuir* 28, 13105–13111.
- Tanaka, A., Sakaguchi, S., Hashimoto, K., Kominami, H., 2013. Preparation of Au/TiO<sub>2</sub> with metal cocatalysts exhibiting strong surface plasmon resonance effective for photoinduced hydrogen formation under irradiation of visible light. *ACS Catal.* 3, 79–85.
- Tang, Z.-R., Yin, X., Zhang, Y., Xu, Y.-J., 2013. Synthesis of titanate nanotube–CdS nanocomposites with enhanced visible light photocatalytic activity. *Inorg. Chem.* 52, 11758–11766.
- Tapley, G.L.H., Crites, C.-O.L., Bejar, M.G., McGilvray, K.L., Ferreira, J.C.N., Scaiano, J.C., 2011. Dry photochemical synthesis of hydroxalate,  $\gamma$ -Al<sub>2</sub>O<sub>3</sub> and TiO<sub>2</sub> supported gold nanoparticle catalysts. *J. Photochem. Photobiol. A: Chem.* 224, 8–15.
- Tapley, G.L.H., Silvero, M.J., Alejo, C.J.B., Bejar, M.G., McTierman, C.D., Grenier, M., Ferreira, J.C.N., Scaiano, J.C., 2013. Supported gold nanoparticles as efficient catalysts in the solventless plasmon mediated oxidation of *sec*-phenethyl and benzyl alcohol. *J. Phys. Chem. C* 117, 12279–12288.
- Tennakone, K., 1985. Semiconducting and photocatalytic properties of mercuric thiocyanate. *Sol. Energy Mater.* 12, 69–75.
- Tian, C., Zhang, Q., Wu, A., Jiang, M., Liang, Z., Jiang, B., Fu, H., 2012. Cost-effective large-scale synthesis of ZnO photocatalyst with excellent performance for dye photodegradation. *Chem. Commun.* 48, 2858–2860.
- Townsend, T.K., Browning, N.D., Osterloh, F.E., 2012. Nanoscale strontium titanate photocatalysts for overall water splitting. *ACS Nano* 6, 7420–7426.
- Tsai, C.-W., Chen, H.M., Liu, R.-S., Asakura, K., Chan, T.-S., 2011. Ni @ NiO core-shell structure-modified nitrogen-doped InTaO<sub>4</sub> for solar-driven highly efficient CO<sub>2</sub> reduction to methanol. *J. Phys. Chem. C* 115, 10180–10186.
- Tu, W., Zhou, Y., Liu, Q., Tian, Z., Gao, J., Chen, X., Zhang, H., Liu, J., Zou, Z., 2012. Robust hollow spheres consisting of alternating titania nanosheets and graphene nanosheets with high photocatalytic activity for CO<sub>2</sub> conversion into renewable fuels. *Adv. Funct. Mater.* 22, 1215–1221.
- Tu, W., Zhou, Y., Liu, Q., Yan, S., Bao, S., Wang, X., Xiao, M., Zou, Z., 2013. An in situ simultaneous reduction-hydrolysis technique for fabrication of TiO<sub>2</sub>-graphene 2D sandwich-like hybrid nanosheets: graphene-promoted selectivity of photocatalytic-driven hydrogenation and coupling of CO<sub>2</sub> into methane and ethane. *Adv. Funct. Mater.* 23, 1743–1749.
- Tung, V.C., Huang, J.H., Tevis, I., Kim, F., Kim, J., Chu, C.W., Stupp, S.I., Huang, J., 2011. Surfactant-free water-processable photoconductive all-carbon composite. *J. Am. Chem. Soc.* 133, 4940–4947.
- Vass, A., Dudaš, J., Tóth, J., Varma, R.S., 2001. Solvent-free reduction of aromatic nitro compounds with alumina-supported hydrazine under microwave irradiation. *Tetrahedron Lett.* 42, 5347–5349.
- Wajid, A.S., Das, S., Irin, F., Ahmed, H.S.T., Shelburne, J.L., Parviz, D., Fullerton, R.J., Jankowski, A.F., Hedden, R.C., Green, M.J., 2012. Polymer-stabilized graphene dispersions at high concentrations in organic solvents for composite production. *Carbon* 50, 526–534.
- Wang, C., Xie, Z., deKrafft, K.E., Lin, W., 2011. Doping metal-organic frameworks for water oxidation, carbon dioxide reduction, and organic photocatalysis. *J. Am. Chem. Soc.* 133, 13445–13454.
- Wang, G., Wang, X., Liu, J., Sun, X., 2012. Mesoporous Au/TiO<sub>2</sub> nanocomposite microspheres for visible-light photocatalysis. *Chem. Eur. J.* 18, 5361–5366.
- Wang, H., Yan, J., Chang, W., Zhang, Z., 2009. Practical synthesis of aromatic amines by photocatalytic reduction of aromatic nitro compounds on nanoparticles N-doped TiO<sub>2</sub>. *Catal. Commun.* 10, 989–994.
- Wang, J.-L., Wang, C., Lin, W., 2012. Metal-organic frameworks for light harvesting and photocatalysis. *ACS Catal.* 2, 2630–2640.
- Wang, P.-Q., Bai, Y., Luo, P.-Y., Liu, J.-Y., 2013. Graphene–WO<sub>3</sub> nanobelt composite: elevated conduction band toward photocatalytic reduction of CO<sub>2</sub> into hydrocarbon fuels. *Catal. Commun.* 38, 82–85.
- Wang, X., Jiang, H., Liu, Y., Gao, M., 2015. Rapid microwave-assisted hydrothermal synthesis of Sm, N, and P tridoped anatase-TiO<sub>2</sub> nanosheets from TiCl<sub>4</sub> hydrolysis. *Mater. Lett.* 147, 72–74.
- Wang, X., Li, S., Yu, H., Yu, J., Liu, S., 2011. Ag<sub>2</sub>O as a new visible-light photocatalyst: self-stability and high photocatalytic activity. *Chem. Eur. J.* 17, 7777–7780.
- Williams, G., Kamat, P.V., 2009. Graphene-semiconductor nanocomposites: excited-state interactions between ZnO nanoparticles and graphene oxide. *Langmuir* 25, 13869–13873.
- Wojtoniszak, M., Zielinska, B., Chen, X., Kalenczuk, R.J., Borowiak-Palen, E., 2012. Synthesis and photocatalytic performance of TiO<sub>2</sub> nanospheres–graphene nanocomposite under visible and UV light irradiation. *J. Mater. Sci.* 47, 3185–3190.
- Wu, J., Shen, X., Jiang, L., Wang, K., Chen, K., 2010. Solvothermal synthesis and characterization of sandwich-like graphene/ZnO nanocomposites. *Appl. Surf. Sci.* 256, 2826–2830.
- Wu, P., He, C., Wang, J., Peng, X., Li, X., An, Y., Duan, C., 2012. Photoactive chiral metal-organic frameworks for light-driven asymmetric  $\alpha$ -alkylation of aldehydes. *J. Am. Chem. Soc.* 134, 14991–14999.
- Wu, S., Yin, Z., He, Q., Huang, X., Zhou, X., Zhang, H., 2010. Electrochemical deposition of semiconductor oxides on reduced graphene oxide-based flexible, transparent, and conductive electrodes. *J. Phys. Chem. C* 114, 11816–11821.
- Xiang, Q., Yu, J., 2013. Graphene-based photocatalysts for hydrogen generation. *J. Phys. Chem. Lett.* 4, 753–759.
- Xie, M.-H., Yang, X.-L., Zou, C., Wu, C.-D., 2011. A Sn<sup>IV</sup>-porphyrin-based metal-organic framework for the selective photooxygenation of phenol and sulfides. *Inorg. Chem.* 50, 5318–5320.
- Xu, T., Zhang, L., Cheng, H., Zhu, Y., 2011. Significantly enhanced photocatalytic performance of ZnO via graphene hybridization and the mechanism study. *Appl. Catal. B – Environ.* 101, 382–387.
- Yang, M.-Q., Weng, B., Xu, Y.-J., 2013. Improving the visible light photoactivity of In<sub>2</sub>S<sub>3</sub>-graphene nanocomposite via a simple surface charge modification approach. *Langmuir* 29, 10549–10558.
- Yang, Z., Xu, X., Liang, X., Lei, C., Wei, Y., He, P., Lv, B., Ma, H., Lei, Z., 2016. MIL-53(Fe)-graphene nanocomposites: efficient visible-light photocatalysts for the selective oxidation of alcohols. *Appl. Catal. B – Environ.* 198, 112–123.
- Yin, Z., Wu, S., Zhou, X., Huang, X., Zhang, Q., Boey, F., Zhang, H., 2010. Electrochemical deposition of ZnO nanorods on transparent reduced graphene oxide electrodes for hybrid solar cells. *Small* 6, 307–312.
- Yu, H., Liu, L., Wang, X., Wang, P., Yu, J., Wang, Y., 2012. The dependence of photocatalytic activity and photoinduced self-stability of photosensitive AgI nanoparticles. *Dalton Trans.* 41, 10405–11411.
- Zen, J.-M., Liou, S.-L., Kumar, A.S., Hsia, M.-S., 2003. An efficient and selective photocatalytic system for the oxidation of sulfides to sulfoxides. *Angew. Chem. Int. Ed.* 42, 577–579.
- Zhan, G., Huang, J., Du, M., Sun, D., Abdul-Rauf, I., Lin, W., Hong, Y., Li, Q., 2012. Liquid phase oxidation of benzyl alcohol to benzaldehyde with novel uncalcined bioreduction Au catalysts: high activity and durability. *Chem. Eng. J.* 187, 232–238.
- Zhang, H., Lv, X., Li, Y., Wang, Y., Li, J., 2010. P25-graphene composite as a high performance photocatalyst. *ACS Nano* 4, 380–386.
- Zhang, J., Xiong, Z., Zhao, X.S., 2011. Graphene–metal–oxide composites for the degradation of dyes under visible light irradiation. *J. Mater. Chem.* 21, 3634–3640.
- Zhang, N., Fu, X., Xu, Y.-J., 2011a. A facile and green approach to synthesize Pt@CeO<sub>2</sub> nanocomposite with tunable core-shell and yolk-shell structure and its application as a visible light photocatalyst. *J. Mater. Chem.* 21, 8152–8158.

- Zhang, N., Liu, S., Fu, X., Xu, Y.-J., 2011b. A simple strategy for fabrication of “Plum-Pudding” type Pd @ CeO<sub>2</sub> semiconductor nanocomposite as a visible-light-driven photocatalyst for selective oxidation. *J. Phys. Chem. C* 115, 22901–22909.
- Zhang, N., Yang, M.-Q., Tang, Z.-R., Xu, Y.-J., 2013. CdS–graphene nanocomposites as visible light photocatalyst for redox reactions in water: a green route for selective transformation and environmental remediation. *J. Catal.* 303, 60–69.
- Zhang, N., Yang, M.-Q., Tang, Z.-R., Xu, Y.-J., 2014. Toward improving the graphene–semiconductor composite photoactivity via the addition of metal ions as generic interfacial mediator. *ACS Nano* 8, 623–633.
- Zhang, N., Zhang, Y., Pan, X., Fu, X., Liu, S., Xu, Y.-J., 2011c. Assembly of CdS nanoparticles on the two-dimensional graphene scaffold as visible-light-driven photocatalyst for selective organic transformation under ambient conditions. *J. Phys. Chem. C* 115, 23501–23511.
- Zhang, N., Zhang, Y., Pan, X., Yang, M.-Q., Xu, Y.-J., 2012. Constructing ternary CdS–graphene–TiO<sub>2</sub> hybrids on the flatland of graphene oxide with enhanced visible-light photoactivity for selective transformation. *J. Phys. Chem. C* 116, 18023–18031.
- Zhang, Q., He, Y.Q., Chen, X.G., Hu, D.H., Li, L.J., Yin, T., Ji, L. L., 2011. Structure and photocatalytic properties of TiO<sub>2</sub>-graphene oxide intercalated composite. *Chin. Sci. Bull.* 56, 331–339.
- Zhang, X., Ke, X., Zhu, H., 2012. Zeolite-supported gold nanoparticles for selective photooxidation of aromatic alcohols under visible-light irradiation. *Chem. Eur. J.* 18, 8048–8056.
- Zhang, Y., Tang, Z.-R., Fu, X., Xu, Y.-J., 2011. Engineering the unique 2D mat of graphene to achieve graphene-TiO<sub>2</sub> nanocomposite for photocatalytic selective transformation: what advantage does graphene have over its forebear carbon nanotube? *ACS Nano* 5, 7426–7435.
- Zhang, Y., Zhang, N., Tang, Z.-R., Xu, Y.-J., 2012a. Graphene transforms wide band gap ZnS to a visible light photocatalyst. The new role of graphene as a macromolecular photosensitizer. *ACS Nano* 6, 9777–9789.
- Zhang, Y., Zhang, N., Tang, Z.-R., Xu, Y.-J., 2012b. Improving the photocatalytic performance of graphene–TiO<sub>2</sub> nanocomposites via a combined strategy of decreasing defects of graphene and increasing interfacial contact. *Phys. Chem. Chem. Phys.* 14, 9167–9175.
- Zhao, J., Zheng, Z., Bottle, S., Chou, A., Sarina, S., Zhu, H., 2013. Highly efficient and selective photocatalytic hydroamination of alkynes by supported gold nanoparticles using visible light at ambient temperature. *Chem. Commun.* 49, 2676–2678.
- Zhao, X., Zhou, S., Jiang, L.-P., Hou, W., Shen, Q., Zhu, J.-J., 2012. Graphene–CdS nanocomposites: facile one-step synthesis and enhanced photoelectrochemical cytosensing. *Chem. Eur. J.* 18, 4974–4981.
- Zheng, Z., Chen, C., Bo, A., Zahir, F.S., Waclawik, E.R., Zhao, J., Yang, D., Zhu, H., 2014. Visible-light-induced selective photocatalytic oxidation of benzylamine into imine over supported Ag/AgI photocatalysts. *ChemCatChem* 6, 1210–1214.
- Zhou, X., Liu, G., Yu, J., Fan, W., 2012. Surface plasmon resonance-mediated photocatalysis by noble metal-based composites under visible light. *J. Mater. Chem.* 22, 21337–21354.
- Zhu, B., Lazar, M., Trewyn, B.G., Angelici, R.J., 2008. Aerobic oxidation of amines to imines catalyzed by bulk gold powder and by alumina-supported gold. *J. Catal.* 260, 1–6.
- Zhu, C., Guo, S., Wang, P., Xing, L., Fang, Y., Zhai, Y., Dong, S., 2010. One-pot, water-phase approach to high-quality graphene/TiO<sub>2</sub> composite nanosheets. *Chem. Commun.* 46, 7148–7150.
- Zhu, H., Ke, X., Yang, X., Sarina, S., Liu, H., 2010. Reduction of nitroaromatic compounds on supported gold nanoparticles by visible and ultraviolet light. *Angew. Chem. Int. Ed.* 49, 9657–9661.
- Zou, R., Zhang, Z., Yu, L., Tian, Q., Chen, Z., Hu, J., 2011. A general approach for the growth of metal oxide nanorod arrays on graphene sheets and their applications. *Chem. Eur. J.* 17, 13912–13917.